# Thin Film PbS Quantum Dot Solar Cells

by

**Matthew Duff**

B.S., University of Pittsburgh, 2015

Submitted to the Graduate Faculty of the

Swanson School of Engineering in partial fulfillment

of the requirements for the degree of

Doctor of Philosophy

University of Pittsburgh

2019

UNIVERSITY OF PITTSBURGH

SWANSON SCHOOL OF ENGINEERING

This dissertation was presented

by

**Matthew Duff**

It was defended on

October 22, 2019

and approved by

Markus Chmielus, PhD, Associate Professor
Department of Mechanical Engineering and Materials Science

Ian Nettleship, PhD, Associate Professor
Department of Mechanical Engineering and Materials Science

Minhee Yun, PhD, Associate Professor, Department of Electrical and Computer Engineering

Dissertation Director: Jung-Kun Lee, Professor
Department of Mechanical Engineering and Materials Science

**Thin film PbS Quantum Dot Solar Cells**

Matthew Duff, PhD

University of Pittsburgh, 2019

The charge carrier kinetics of P and N type Lead sulfide quantum dots were examined to determine metrics for hole and electron transport during solar cell operation. This was achieved by using a dual illumination scheme to excite the solar cell through front and back contacts. By changing the illumination direction, the distances hole and electrons travel will also be switched. This allows us to measure the carrier kinetics of the farthest moving charge carrier during solar cell operation. Using JV, IPCE, and current decay measurements, this study found that hole and electron transport in N type PbS is symmetric. In P type PbS, electron transport suffers compared to hole transport. With the addition of a P/N junction in the active layer, the transit times for both holes and electrons decreased significantly with large improvements in carrier transport.

Tamm surface plasmons were investigated to determine their effect on the optoelectronic properties of PbS quantum dot solar cells. Tamm surface plasmons form when a Bragg mirror is in contact with a thin metal film. Strong plasmonic resonances occur in the metal film for photons with the same wavelength as the Bragg wavelength. When put in conjunction with a PbS solar cell, the plasmonic film enhanced the light absorption of the device leading to more photon absorption and charge generation, improving the efficiency of the PbS quantum dot solar cell. Light absorption was improved through near and far field plasmonic effects. Near field effects coupling light to the gold film greatly increasing the optical cross section of PbS near the thin film for photons near the Bragg wavelength. Far field effects increase the optical pathway in the PbS film. Different wavelength of light can be targeted by the Tamm surface plasmon effect by changing the

dielectric layer thicknesses of the underlying Bragg mirror. This research can be applied to other solar cell types to acquire qualitative information on hole and electron transport. Tamm surface plasmons are an understudied topic in the field of plasmonic assisted solar cell design and this paper can act as a stepping stone for future research.

## Table of Contents

## List of Tables

## List of Figures

## Acknowledgements

This research is the culmination of years of trial and error with more failure than success. The contents have been presented at conferences and two pending paper. Through my failures, I could learn more about my research as well as myself. Persistence has helped me finally finish.

I could not have complete the task of finishing my studies alone. I would firstly like to thank my advisor, Dr. Lee, for his patience, support, and perseverance to help me finish my experiments and analyze my data. Without his mentorship, I would still be meandering trying to even find my research goals. I would like to thank my committee members for their suggestions for improving my research as well as donating their time to review and critique my project.

My lab mates: Fen Qin, Seongha Lee, Fanda Yu, Sumin Bae, Dr. Gill Sang Han, Dr. Youngsoo Jung, Dr. Heesuk Roh, Dr. Poshun Huang, and Dr. Salim Caliskan. Thank you for your help with the finer details of making my experiments a reality.

I would like to thank Lauren for her unwavering support and belief in me even when I didn't believe in me. Thanks Mom for everything for your support throughout my academic career. Thanks to my whole family for their constant presence in my life. I owe a lot to my ancestors who left their homeland to come to America for a better life. This country will always be a country of immigrants.

# 1.0 Introduction

The shift from fossil fuels to renewable energy sources to supply humanity with energy has been part of a multidecade research push to generate inexpensive electricity, reduce $CO_2$ output, and combat global climate change. [1-6]

Photovoltaic devices are a type of renewable energy system that have dominated new research in alternative energy. Simply put, photovoltaic devices convert solar energy in the form of photons to usable electrical energy.[7] Interest in efficient and inexpensive photovoltaics come is due to the large amount of solar energy hitting the earth from the sun as well as the low maintenance costs of photovoltaics. There are many types of materials in photovoltaic devices that absorb energy. The clear leading absorber material in photovoltaic devices has been silicon type solar cells.[8] Si solar cells combine high light absorption and low charge recombination to absorb the majority of solar irradiation while efficiently transporting generated charges outside of the solar cell. [9] The primary metrics for solar cells are the ability for the absorbing layer to capture solar light and convert photons to electron-hole pairs and then to transport the generated electrons and holes out of the solar cell to produce useful electrical work.

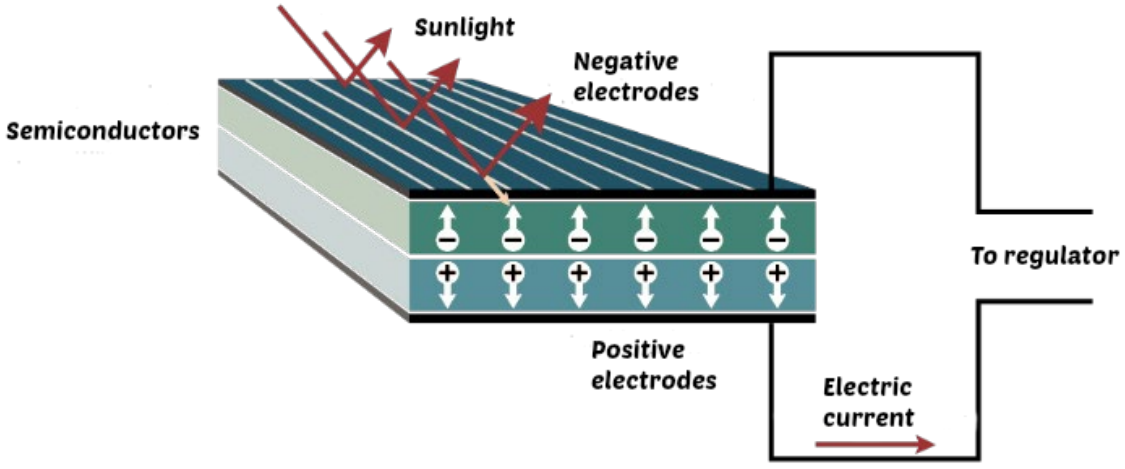


**Figure 1 Shows semiconductor absorbing light and electrons and holes being transported [2]**

While Si has been largely successful in solar cell devices, other semiconducting materials have been investigated because Si is expensive to produce.[8] PbS quantum dot devices have been studied because they are fabricated without using expensive fabrication techniques and have a higher theoretical efficiency than Si devices.[10, 11] PbS quantum dots can absorb light to through multiple excitation generation. [12, 13]A process that can produce two electrons for every one absorbed photon if the energy of the photon is twice that of the band gap of the PbS film. This is in contrast to tradition semiconductors where one photon can only generate one electron and any excess energy is lost to heat. Therefor the theoretical efficiency of PbS solar cells is ~45% whereas Si solar cells is only ~30%. Even though the theoretical efficiency is so high, actual fabricated lab devices have only achieved a record efficiency of 13%.[14] The difference is theoretical and actual device efficiency is due to the poor charge transport properties of PbS semiconductor films.

## 1.1 Solar cell physics

Solar cells are semiconductor devices that allow for the direct conversion of energy stored in a photon to energy stored in an electron.[9, 15] The separation of electronic bands in the semiconductor allow this phenomenon to happen. In a semiconductor there is a conduction band and a valence band as shown below.[16, 17] These bands are the allowed electron energy states defined by the quantum mechanical wave function. The electron distribution and band energy is intrinsic to each material as it is controlled by crystal structure and atomic bonding types.

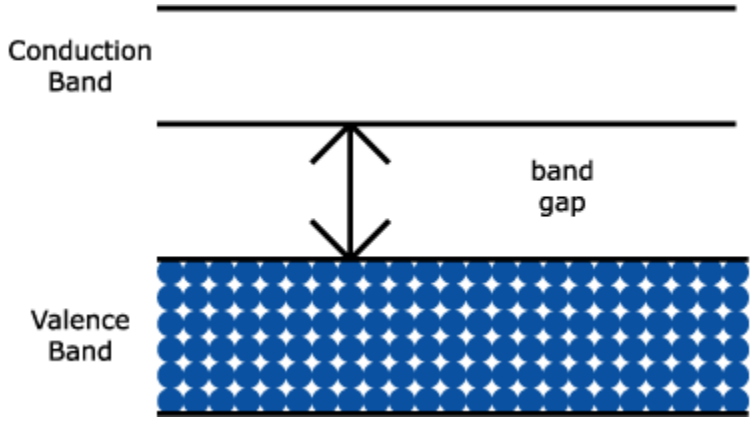


**Figure 2 Valence and conduction band of semiconducting solids [18]**

For an intrinsic semiconductor, the valence band is completely filled and the conduction band is empty. The band gap is the energy difference between the conduction and valence band. It is in this region, also known as the forbidden region, electrons are forbidden to enter as there are no valid energy states in that zone. For a valence band electron to be promoted to the conduction band, a quantum of energy must be imparted to it at least as large as the value of the energy gap. In solar cells, photons can be absorbed by the semiconductor to produce an excited electron as well as a hole. It must be noted that if a photon with an energy lower than the band gap strikes the

semiconductor it will not be absorbed as electrons cannot be in the forbidden region. All electrons that are excited to the conduction band have approximately the same energy, this is due to the fact that if an electron has a higher energy that the conduction band, it will lose energy until it is at the conduction band minimum. This process is called thermal decay. For a quantum dot however, the electron decay process is a little different. If a phonon is absorbed by the PbS with at least twice the energy of the band gap, a second electron can be promoted to the conduction band through a process called multiple excitation generation.[13] The second electron generation will increase the amount of current that a solar cell is capable of producing.

Once charges are produced however, they must be transported out of the solar cell into an external circuit to do work. During charge transport, the excited charges tend to lose their energy and return to the ground state. This process is called recombination and any energy absorbed by the solar cell is lost as heat. Solar cell design and fabrication is heavily focused on reducing recombination. Recombination is exacerbated by the presence of defects in a solar cell such as vacancies or grain boundaries. These defects are obstacles for charge transport and reduce overall device efficiency. The recombination of solar cells can also be reduced by decreasing the thickness of a solar cell. If the solar cell thickness is small, the charges will not have to travel far, reducing the probability of coming in contact with a defect and reducing the probability of recombination. [19]

This principle of reducing absorber film thickness to improve charge transport comes with a tradeoff however, if the absorber layer is thin, the layer cannot absorb the majority of light hitting the semiconductor and most photons will pass through. If the absorber layer is too thick, all of the light will be absorbed and the solar cell will have a high charge generation however because the charges have to travel the width of the thick film, most of the charges will recombine with the

energy being lost to heat. For both cases, device efficiency will be low and the optimum device design is somewhere in the middle. There is a trade-off between light absorption and carrier transport in traditional solar cell device architectures.

## 1.2 Quantifying solar cell Performance

### 1.2.1 Current-Voltage measurements

A solar cell's efficiency is the ratio of extracted electrical power to incident solar power. To measure a solar cell's efficiency current-voltage measurements are used.[20] A voltage sweep is applied to the solar cell under illumination and the resulting current is measured. The maximum product of voltage and current is the maximum power point of the solar cell dividing this power point by the amount of known optical power supplied to the device by the light source will give the efficiency. The main metrics used for IV measurements are the short circuit current density (Jsc), open circuit voltage (Voc) and fill factor.

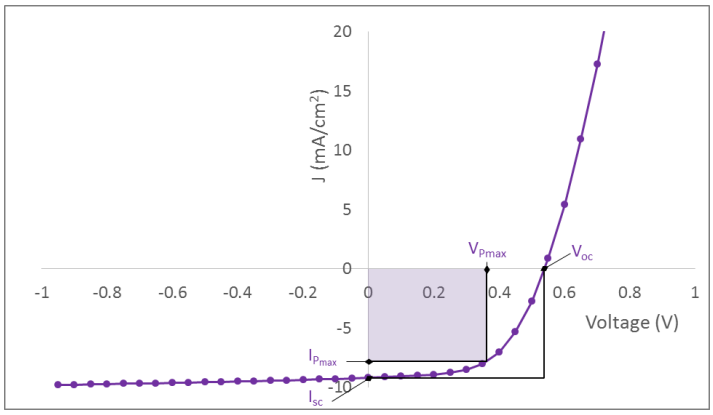


**Figure 3 Example IV curve of a solar cell. Metrics pointed out are the Voc, Isc and the maximum power point.**

The open circuit voltage of the solar cell is the maximum voltage that the solar cell will supply; that is the voltage without any load applied. The short circuit current of a solar cell is the maximum current of the solar under conditions of a zero-resistance load; a free flow or zero volt potential drop across the cell. The issue with the two states, Jsc and Voc, is that the most interesting aspect of a solar cell is not the flow with no potential drop, nor the potential drop with no flow, but the product of these two; the power. When either the potential drop or the current flow is zero, the power being the product of the two will be zero. Therefore, a more interesting aspect is the maximum power and how large the maximum power is in respect to the product of the Voc and Isc. This term is what is referred to as the fill factor. The ratio between the maximum power represented by figure 3 and the full square spanned by the Voc and Isc values. This simple test gives broad information on the overall device performance of the solar cell.

The equivalent circuit of the solar cell is a diode in parallel with a current source and a resistor that is also in series with a resistor shown in figure 4.[21]

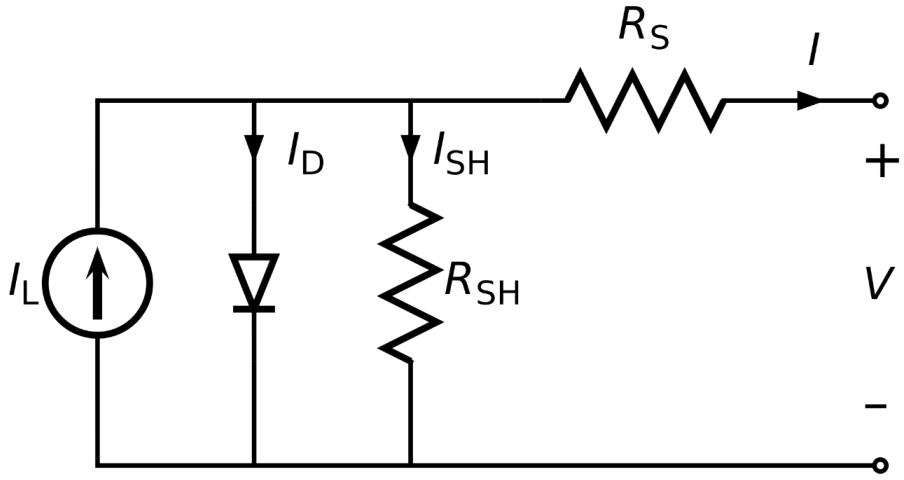


**Figure 4 equivalent circuit of a generic solar cell. In parallel is a current source, diode, and Shunt resistor in series with the series resistor.**

Il is the current source, this represents the active layer of the solar cell as it generates charges from sunlight. Id is the diode of the solar cell that give directionality to generated charges. Rs and Rsh are the series and shunt resistances and are a more of a composite metric. The shunt resistance represents ways current could flow around the diode in the physical form of holes in films or defects in doping.[22-27] Ideally this value should approach infinity as directionality of current is important for efficient solar cell operation. The series resistance represents all parasitic resistances in a device and they physical meaning varies depending on device structure.[21, 26, 28-30] For the most party, these are defects in fabrication that act as recombination centers for holes and electrons. The increase in recombination reduces the extracted current and decreases the overall performance of the device. Ideally this value should be zero and charge transport in the device will be perfect with no energy loss due to heat.

### 1.2.2 IPCE (incident photon conversion efficiency)

IPCE or Quantum Efficiency (QE) is a measure of how efficiently the device converts the incident light into electrical energy at a given wavelength.[31-34] The principle of EQE measurement is based on illuminating the sample by a monochromatic light and recording the device electrical current (number of generated carriers). The quantum efficiency values are a combination between absorption of light and charge transport. The quantum efficiency measurement is a probability that a photon of a specific wavelength will be absorbed to produce and energetic electron/hole. Next the electron and hole must be extracted to the external circuit to do work. The probability of recombination decreases the quantum efficiency probability.

The equation of quantum efficiency is shown as

$$\mathrm{EQE} = \frac{\text{electrons/sec}}{\text{photons/sec}} = \frac{(\text{current})/(\text{charge of one electron})}{(\text{total power of photons})/(\text{energy of one photon})} \tag{1.1}$$

By varying the frequency of the light the entire curve of the current as a function of wavelength can then be established.

To measure real devices and to reduce error from light intensity that may differ between experiments and the distribution of energy across measured wavelengths, the data for each run is compared to a reliable reference cell whose IPCE is known. These reference devices do not significantly change over time and are commercially produced Si, Ge, or GaAs device. To calculate the IPCE using real measurable metrics, the equation becomes:

$$EQE = \frac{1240\ eV/nm}{wavelength(nm)} * \frac{(sample\ current)(responsivity)}{Reference\ cell\ current} \quad (1.2)$$

The formula first determines the energy per photon at the measured wavelength. Then divides the measured current from the sample by the current from the known reference cell. Finally, the responsivity is a property that is intrinsic to the known reference cell and is a measure of the IPCE of the reference cell.

Figure 5 shows an example of an EQE curve for a typical P3HT:PCBM based device. The area under the curve will then represent the total number of carriers created by the device under full spectrum white light illumination. In other words, the integration of the curve will give the electrical current density.

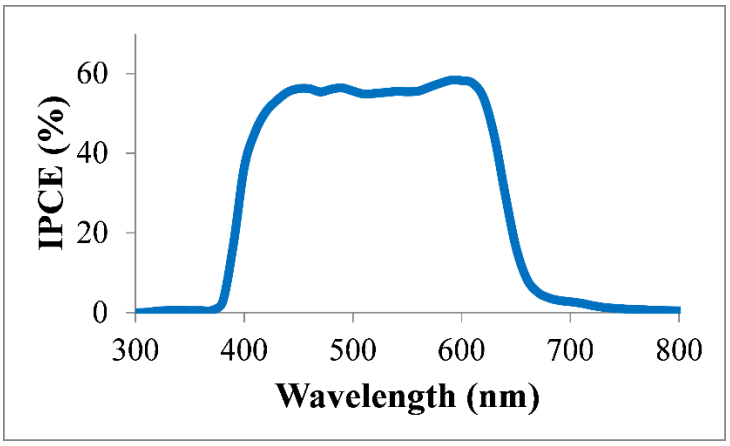


**Figure 5 Incident Photon to Charge Carrier Efficiency as a function of wavelength for typical Organic Solar cell device.**

### 1.2.3 Transient Current and voltage decay

It is important to measure the photo generated carrier lifetime in the solar cell, since the carrier transport kinetics play a large role in determining the conversion efficiency of the device.[35-42] So far, two methods have been mainly used in electron lifetime characterization, including open circuit voltage decay (OCVD) and stepped light-induced transient measurements of photocurrent and photovoltage (SLIM-PCV).[43]

OCVD is a powerful and simple tool to measure the electron lifetime of the DSSCs as a function of the photovoltage (*Voc*). This method consists of turning off the illumination in a steady state and monitoring the subsequent photovoltage decay.108 It provides a continuous reading of the lifetime change against the *Voc*, and the data treatment based on the carrier recombination mechanisms is quite simple. Figure 6 shows the measurement setup. Monochromatic laser beam with an instant turning off at a steady state is generated from a laser diode (λ=660 nm) which is controlled by a function generator. A voltage decay from the steady state is monitored by a digital storage oscilloscope that is synchronized with the function generator.

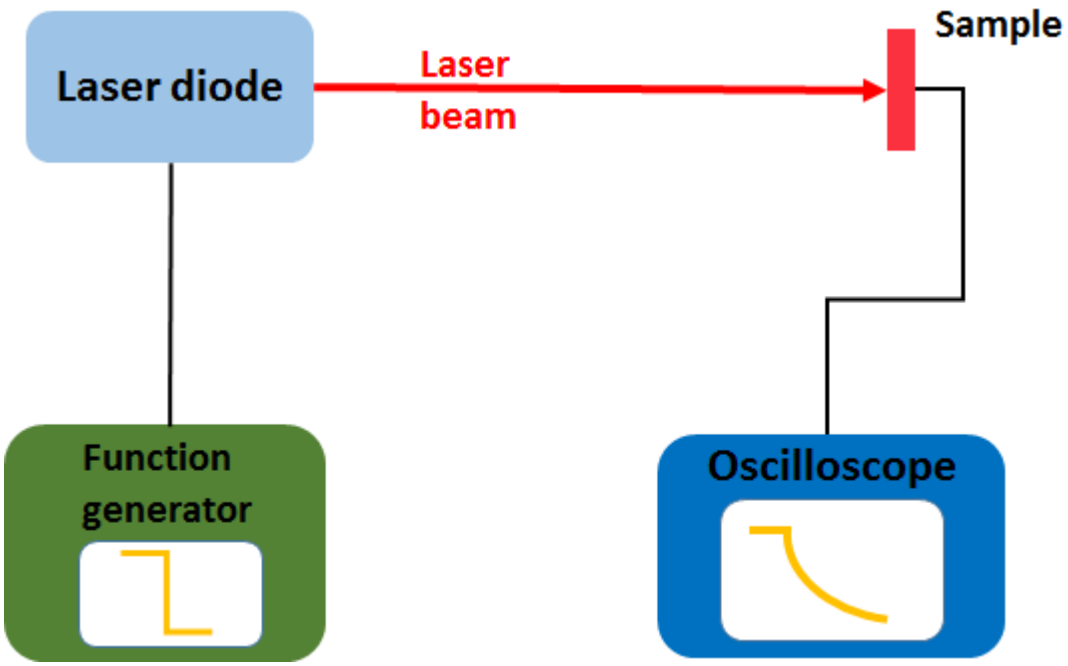


**Figure 6 Set up of open circuit voltage decay measurements**

The electron lifetime is theoretically derived from a general recombination rate, which involves a higher reaction order charge transportation mediated by internal trapping and de-trapping processes. For a common nonlinear case, the electron lifetime is given by the reciprocal of the derivative of the decay curve normalized by the thermal voltage. [44-46]

$$\tau_n = -\frac{k_B T}{e}\left(\frac{dV_{OC}}{dt}\right)^{-1} \tag{1.3}$$

In the set up shown in figure 5, measures the change in voltage at open circuit voltage conditions due to a change in light intensity. At open circuit voltage conditions, there is no current flow out of the cell. The residual voltage change is due to how long the charges remain stable without being replenished by a high generation rate.[47]

Typical results shown in Figure 7 consist of OCVD decay curves at different light intensities and SLIM-PCV can simplify the optical setup and reduce the measurement time in comparison to conventional time-of-flight and frequency-modulated measurement. It is a perturbation measurement applying a stepwise change in light intensity and monitor the change of photocurrent and voltage under this perturbation. Both electron diffusion coefficient and lifetime can be obtained from the SLIM-PCV measurement.[48] The experimental setup is shown in Figure 3-3. Monochromatic laser beam with a step change of intensity was generated from the laser diode ($\lambda$=660 nm) which is controlled by the function generator. A set of neutral density (ND) filter was used to change the laser intensity and placed in front of the sample. Voltage transient was monitored by the oscilloscope that is synchronized with the function generator. And current transient was obtained from the oscilloscope through a current amplifier, which can convert current signal into voltage signal. The oscilloscope again measures a voltage change from the change in light intensity and therefore charge generation rate. However, the voltage is recorded from a current amplifier that measured the change in current from the sample due to the change in light intensity. Due to this, the measurements of open circuit voltage measurements have a different meaning compared to open circuit voltage measurements. Since charges are moving, this measurement has more weight based on the kinematics of charge transport.

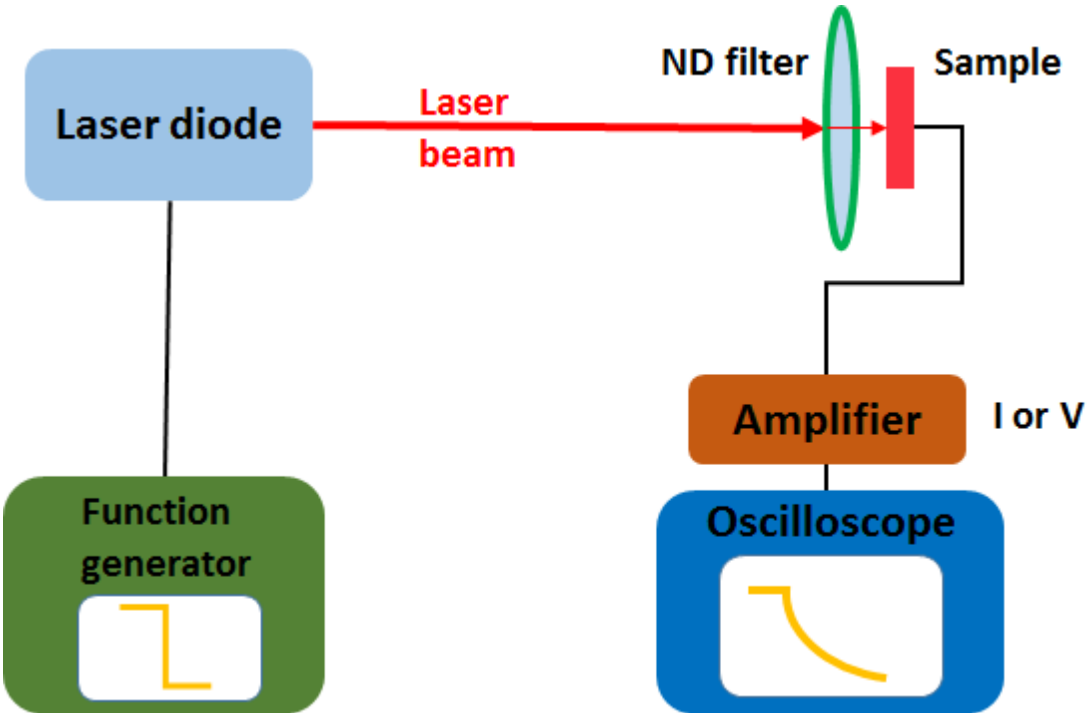


**Figure 7 Short Circuit current decay experimental set up**

At a short circuit condition of the solar cell, initial light intensity, which corresponds to the short circuit current (*Jsc*), drops to a constant value instantly. This sudden reduction of partial light intensity induces the current transient. The time to reach the constant current value depends on the electron diffusion coefficient, which can be expressed as [43]

$$D = L^2/(2.77\tau_C) \tag{1.4}$$

where L is the thickness of the electrode, and $\tau_C$ is the exponential decay time constant.

The electron lifetime is measured from the photovoltage response of the DSSCs against the perturbation of light intensity at the open circuit condition. The electron density has the following relation

$$n(t) = Aexp(-t/\tau) \tag{1.5}$$

Where A is Δn, the difference of electron densities before and after the light intensity change.109 Under the small perturbation of light intensity, *Voc* should be proportional to equation 3-3. Thus, the carrier lifetime can be derived from fitting of the relaxation time of the open circuit voltage decay. Typical current responses and open circuit voltage transients as a function of time are shown in Figure 8.

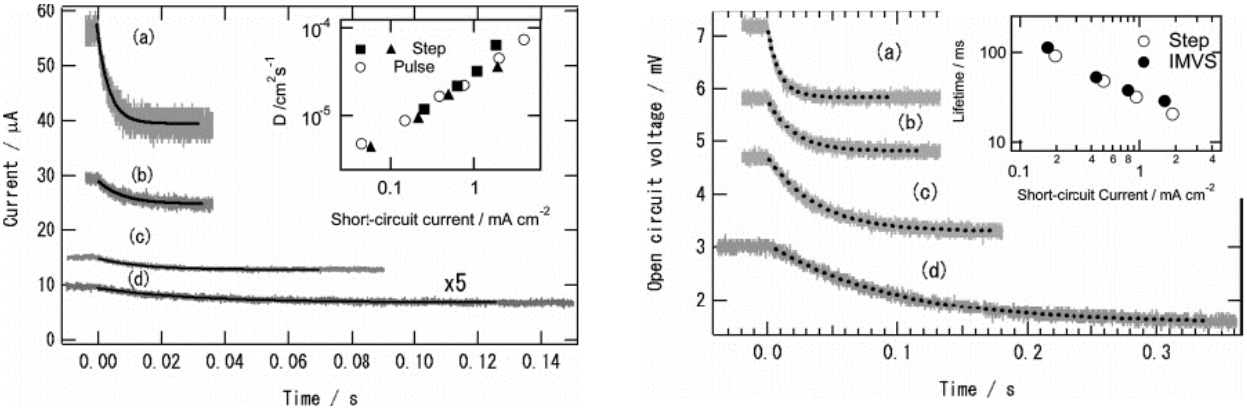


**Figure 8 Transient current and voltage measurements found through the SLIM method**

## 1.3 Quantum Dot Solar Cells: State of the Art and limitations

The purpose of PbS solar cells is to convert solar energy into electrical energy through the photoelectric effect. A photon hits the solar cell to generate a free electron that can then do work in an external circuit without consuming natural resources to operate. For PbS solar cells, PbS quantum dots absorb light.

Quantum dots are simply nanoscale particles (less than 10's of nanometers) where the energy levels of electrons change depending on the size of the particle due to a phenomenon called quantum confinement.[49-52] The size, and therefore the energy levels, of the quantum dot can be tuned to fit the specific application e.g. for large quantum dots, the energy it takes to free an electron is small so it can absorb most solar energy even low energy photons. However, the free electrons do not have enough energy to be used in an external circuit. Quantum dots for power generation employ small quantum dots that will absorb less of the solar spectrum but have more energetic free electrons.

Quantum dot solar cells are researched for both scientific and economic reasons.[53] Quantum dots exhibit a phenomenon called multiple excitation generation.[13, 52, 54-57] For traditional semiconductors, when a photon is absorbed only one free electron is produced no matter how much energy that photon has. The energy difference between how much energy it took to free the electron and the energy the photon had is lost as heat. For quantum dots however, that excess energy can be used to excite another electron which in turn increases the current generated by the device. This phenomenon pushes the theoretical limit of efficiency for a single absorber solar cells. PbS quantum dos are also direct band gap semiconductors. From this, their light absorption coefficient is much higher than indirect band gap semiconductors such as silicon. A PbS absorbing

layer can be much thinner than Si, requiring less material to produce a sufficiently thick film to absorb the majority of light.

### 1.3.1 Quantum dot fabrication

Economically, PbS quantum dot solar cells are less expensive to fabricate compared to traditional silicon solar cells due to lower fabrication temperatures, purity requirements, and inexpensive precursors. PbS quantum dots are fabricated through wet chemistry and devices are fabricated with solution processing methods such as spin coating or spraying at room temperature. PbS quantum dots can be dispersed in organic solvents, the solvents are coated on a substrate and then evaporated. After evaporation, the PbS quantum dots remain in a film. To control the thickness of the film, the concentration of PbS, the type of solvent, and lastly, the number of deposition cycles can be controlled. [11, 58-63]

Despite these advantages, PbS quantum dot solar cells currently have no industrial application as a power generation device due to its poor efficiency. Commercial Si solar cells have an efficiency of around 25% were as the best lab fabricated PbS device is 11.8%. [14]

### 1.3.2 Quantum dot film charge transport

This large difference in efficiency is primarily due to the conduction mechanism in quantum dot films. [35, 64-66] Because a quantum dot film is comprised of a stack of individual quantum dots, there is a small discontinuity between each quantum dot. The film can be thought of as a nano-crystalline solid where each “grain boundary” between the PbS quantum dots is a barrier for charge transport and potential recombination center. These “grain boundaries are

intrinsic to PbS quantum dot devices as small nanoparticles are necessary for quantum confinement to occur. Without quantum confinement, the energy levels in the PbS film will not be compatible with solar cell devices.

Because the quantum dot film is comprised of a lot of nanoparticles the conduction mechanism is through charge hopping. Charges must hop from one quantum dot to the next and the conductivity is inversely proportional with inter-quantum dot spacing. As quantum dots become father apart, the barrier for charge transport becomes higher and the probability of recombination becomes high. Due to the unique charge transport mechanism, the overall charge transport in the film is worse than devices that can be made from single crystals.[67] With all solar cells, there is a tradeoff between light absorption and carrier transport. However, in PbS quantum dot films, this tradeoff is much more severe due to the unique charge carrier mechanism.

With no surprise, the most effective and cutting edge research has gone into reducing quantum dot spacing. To understand how researchers have done this, it is important to understand quantum dot synthesis and device fabrication. [68]

The first breakthrough in the field PbS quantum dot solar cells was the discovery of how to make stable and uniform PbS quantum dots through simple wet chemistry. Hines and Scholes published a paper in 2003 and accelerated progress in the field as researchers could reliably fabricate high quality quantum dots.[69] The controlled synthesis of quantum dots was facilitated by discovering quantum dots could be fabricated by injecting an organic-sulfur precursor into a lead oleate mixture. The lead oleate mixture is made by dissolving lead oxide in oleic acid and octadecene at temperature of ~120 °C in an inert atmosphere. Lead oxide and oleic acid form lead oleate and water. The water will evaporate and the lead oleate mixture dissolves in octadecene. Upon addition of the sulfur precursor, PbS quantum dots nucleate and crash out of solution as their

solubility decreases. The role of oleic acid is to reduce the interfacial energy between the PbS and octadecene solvent. By adding more oleic acid, it is less thermodynamically favorable for nucleation to occur. Less nucleation sites allow for more growth and larger quantum dots.

The surfaces were capped by the oleate ligands by binding to the lead atoms. The oleate ligands have three main purposes: to stop the growth of the quantum dots, to passivate the surface to inhibit attack from oxygen, and the long carbon chain allows the nanoparticles to be readily dispersed in organic solvents. By modifying injection temperature and oleic acid concentration, size tunable, uniform, and stable quantum dots can be fabricated.

To make more conductive quantum dot films, researchers have focused on using different ligands and techniques to reduce quantum dot separation distance. This has included using short thiols, sulfur-cyanides, and most notably halides.[39, 70-78] During a typical fabrication process, quantum dots with oleate ligands are dispersed in a non-polar volatile solvent such as hexane. The hexane solution is then coated on a metal oxide substrate. After the solvent evaporated, the quantum dots remain. To remove the native oleate ligands, a solution containing the more reactive shorter ligands is dropped on the quantum dot film to replace the long oleate ligands. The excess short ligands and free native ligands are then washed off to complete a process called ligand exchange. For example, to replace the oleate ligand with EDT (1,2-Ethanedithiol a short thiol) a solution of EDT in acetonitrile is dropped on the surface. The Thiol, having a strong bond with heavy metals, replaces the oleate ligand to form a complex with lead. The oleate ligand is dissolved into the acetonitrile and washed away. With the addition of the Thiol based ligands, the PbS quantum exhibits P type behavior. From Stoichiometry, there are more sulfur atoms than lead atoms on the quantum dot the more anions there are, the more holes that need to be generated to maintain charge neutrality.

Using EDT as a ligand has greatly improved PbS solar cell performance as the long native ligands are replaced by short ones. This reduces the quantum dot spacing and the barrier for charge transfer.

The fabrication of N type PbS has been difficult for researchers to make for used in a stable solar cell. Some research strategies have been to use alkali metals to impart N type behavior on the solar cell.[79-82] The alkali metals are not stable on the PbS surface in the presence of water in the air. The solar cell performance of these devices degrade quickly as the alkalis on the surface of the quantum dot are removed and quantum confinement is lost. A breakthrough came when researchers discovered that N type behavior can be impaired to PbS quantum dot solar cell while still maintaining air stability.[11] Their approach is to use atomic iodine as a ligand on the surface of the quantum dot; Iodine has an additional electron $^{-1}$ compared to sulfur $^{-2}$. Due to this extra electron, the film has N type behavior that is stable in air. The iodine replaces the native oleate ligand in the same process as with EDT. Tetrabutylammonium Iodide in methanol is dropped on the surface. In this reaction, the Iodine replaces the oleate ligand in the Pb-oleate bond to form a Pb-I bond on the surface. The oleate ligand binds with the TBA+ molecule and is dissolved into the excess methanol.

Another advantage of using iodine ligands is the overall quantum dot spacing will decrease. The iodine ligand is only one atom which is the minimum ligand size. The creation of N type PbS quantum dot films opens new device architecture and the ability to combine P and N type PbS quantum dot films in the same device. This strategy has been shown to greatly improve quantum dot solar cell performance.

Advancements in device efficiency have been primarily with the development of ligand exchange techniques. The previously discussed solid state ligand exchange procedure still leaves

some un-exchanged oleate ligands on the quantum dot surface. Research has been successful in maximizing the number of iodine ligands on the quantum dot surface through a combination of liquid and solid state exchange procedures.[74] While the quantum dots are still in a nonpolar solvent, iodine salts are dissolved in the solution to “prime” the quantum dots prior to film deposition. Efficiencies for this procedure have increased device performance to over 10%

### 1.3.3 PbS Quantum Dot Light Absorption

The quantum dot absorption spectra are unique compared to traditional semiconductors.[10, 49, 50, 83] The light absorption spectra for traditional semiconductors can be broken into three distinct regions. When photons with energies below the band gap hit the semiconductors, they pass through without getting absorbed. For photons with energies equal or slightly over the band gap, the photons are absorbed but the absorption coefficient is low as there are few allowable transitions from the valence band to the conduction band so the probability for absorption is low. the only transition for electrons at the band gap is the transition from the top of the valance band to the bottom of the conduction band. This transitions is available for one electron orbital. For photons with energies well above the band gap, the absorption coefficient is high as there are more possible transition states. The more possible electron energy transitions, the higher the absorption coefficient. The results of this is an absorption spectra that is 0 at energies below the band gap, then an exponential increase at the band gap followed by a plateau. [64]

Quantum dot absorption spectra are a quite different compared to traditional bulk semiconductors and this is the to the energy levels in the valance and conduction band. As shown in figure 9, the valence and conduction bands are continuous for bulk semiconductors. Through the process of quantum confinement, the energy levels in the quantum dot valance and conduction

bands becomes discrete. The consequence of this is a reduction of allowable electron transition states. The consequences of this are shown in figure 8B. The absorption spectra for quantum dots peaks for photons with energies above the bandgap, the decreases to a minimum, and increases quickly again. Photons with energies at that minima are not readily absorbed because there are few electrons that can make that energy transition. [83]

Poor light absorption is the cause of the IPCE valley in figure 9C. the poor light absorption of the PbS film decreases the carrier collection efficiency at wavelengths where the quantum dots have poor light absorption coefficients. A low IPCE value means the total extracted current is poor leaded to low current densities and poor overall device efficiency.

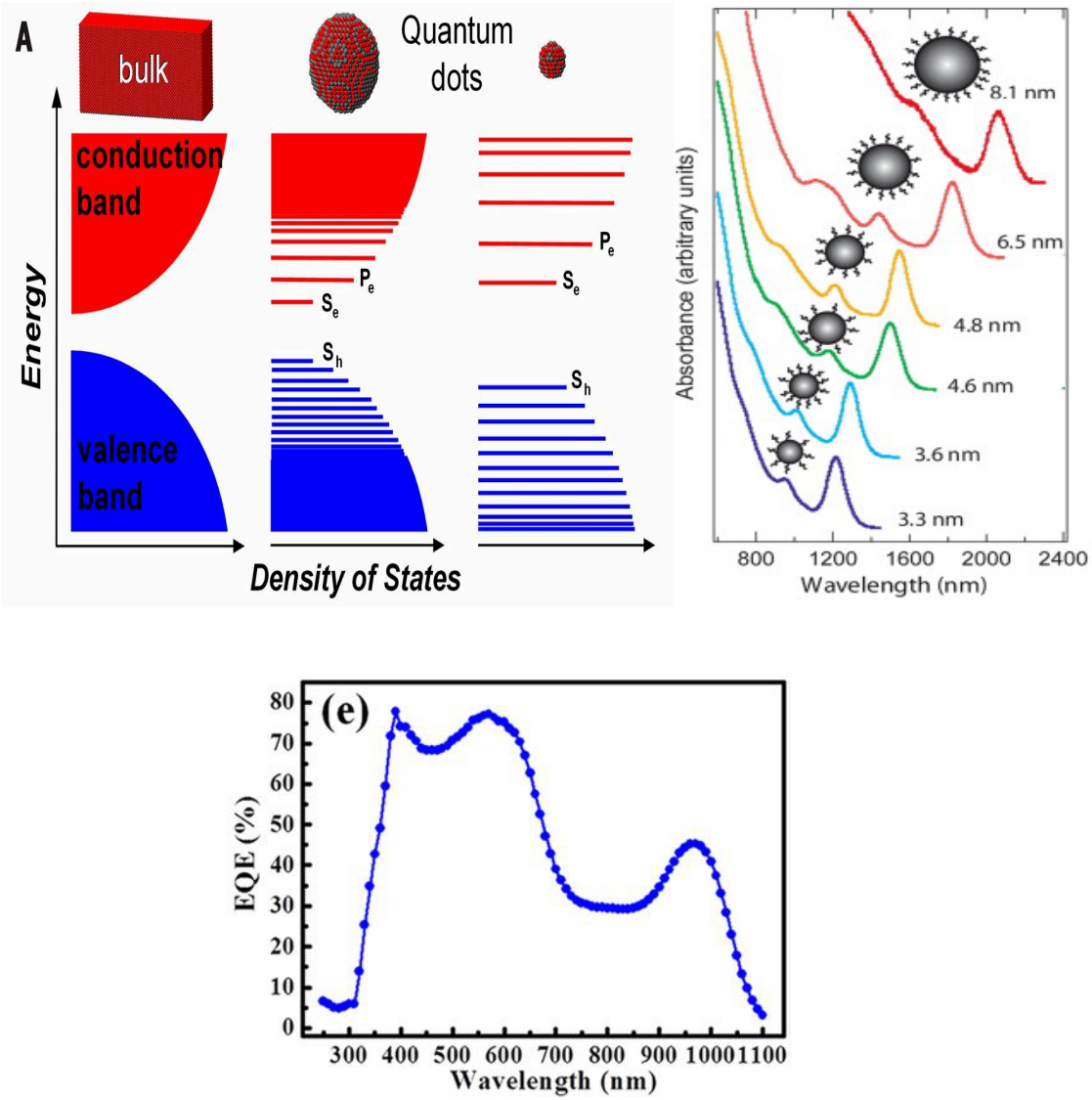


**Figure 9 A) Density of states for bulk and quantum dot materials. the energy levels for bulk are continuous whereas for quantum dots have discrete energy levels. B) due to the discrete energy transitions of the quantum dots, the absorption spectra will have absorption peaks corresponding to the first transition from the valence to the conduction band. C) the consequence for quantum dot solar cell devices is weak light absorption over specific wavelengths. [75]**

Some researchers have tried to increase the light absorbance of the quantum dot film by increasing the quantum dot film thickness. While this strategy increases light absorption, recombination in the device increases as the generated charges must travel further in the quantum dot film to be extracted. This strategy is also inefficient because the absorption coefficient of PbS for most photon wavelengths is high, only certain regions of the quantum dot absorption spectra is low. To increase the light absorption of PbS at those specific wavelengths, surface plasmon be used. By tuning the surface plasmon resonance to affect the PbS quantum dot film at the absorption minima, the charge carrier collection efficiency of the quantum dot devices can be improved. The light absorption properties of the PbS quantum dot film increase without increasing the film thickness so the charge transport properties of the device are not negatively affected.

### 1.3.4 Plasmonics to improve light absorption

Plasmonic nanoparticles have been shown to improve the light absorption properties of semiconductors at specific wavelengths of light when plasmonic nanoparticles are imbedded in the semiconductor film.[84-90] Plasmonic nanoparticles usually are comprised of a thin metal shell or core. The electron plasma of metals can absorb light if the frequency of the light matches the frequency of the electron oscillation in the metal. When light is absorbed, the energy from the photons is converted to electric potential energy and an electric field is formed at the metal surface. the plasmonic phenomenon has been utilized in in the fields of nanofabrication and photovoltaics, and photoelectrical chemical cells.[85-96] My interest in plasmonics is how the surface plasmon effect can be leveraged in PbS quantum dot devices.

Plasmonics can increase the light absorption of semiconductor active layers in photovoltaics through multiple mechanisms shown below in figure 10.

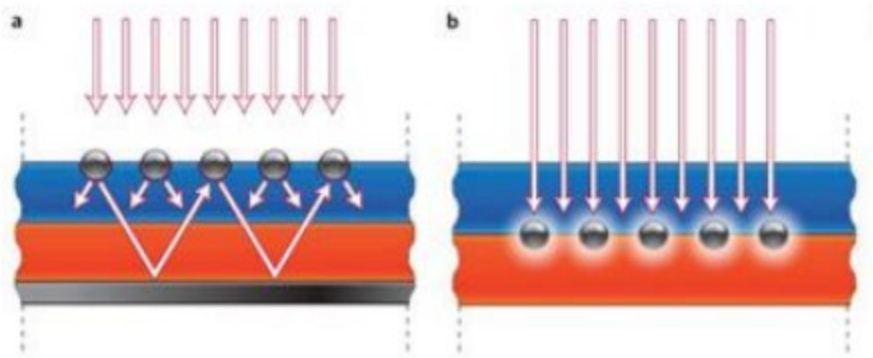


**Figure 10 Two mechanisms in which surface Plasmon resonance increases light absorption in semiconductor by A) increasing the optical pathway photons take in the active layer film and B) light can be trapped by near field coupling to the surface of the metal nanoparticles.**

Utilizing the plasmonic effect in the form of nanoparticles has been a useful tool to improve light absorption in thin film solar cells due to light path folding and electromagnetic field enhancements. Light path folding is due to scattering and reflectance effects from the surface plasmons. Light that is scattered from the surface plasmons are deflected at an angle through the semiconductor film, this increases the optical wave pathway and the optical thickness of the thin film solar cell. This can be seen as a far field effect as its enhancement mostly affects the whole of the semiconductor device. The other mechanism that improves light absorption in thin film solar cells is through electromagnetic field enhancements. [97-100] Light can be trapped by the excitation of surface plasmons on the surface of the metal. This mechanism can be referred to as near field enhancements as the mechanism only affects 10's of nanometers away from the metal surface as the field decays exponentially over distance. This greatly increases the optical cross section of the semiconductor around the plasmonic device allowing for more electrons to be excited in the semiconductor.

To utilize the plasmonic phenomenon in solar cells, metal nanoparticles have been traditionally used. Metal nanoparticles have been placed in direct contact with the semiconducting absorber layer. By adding these metal nanoparticles in solar cell devices the solar collection efficiency of the device can be improved by improving the light absorption properties of the semiconductor shown in figure 11.

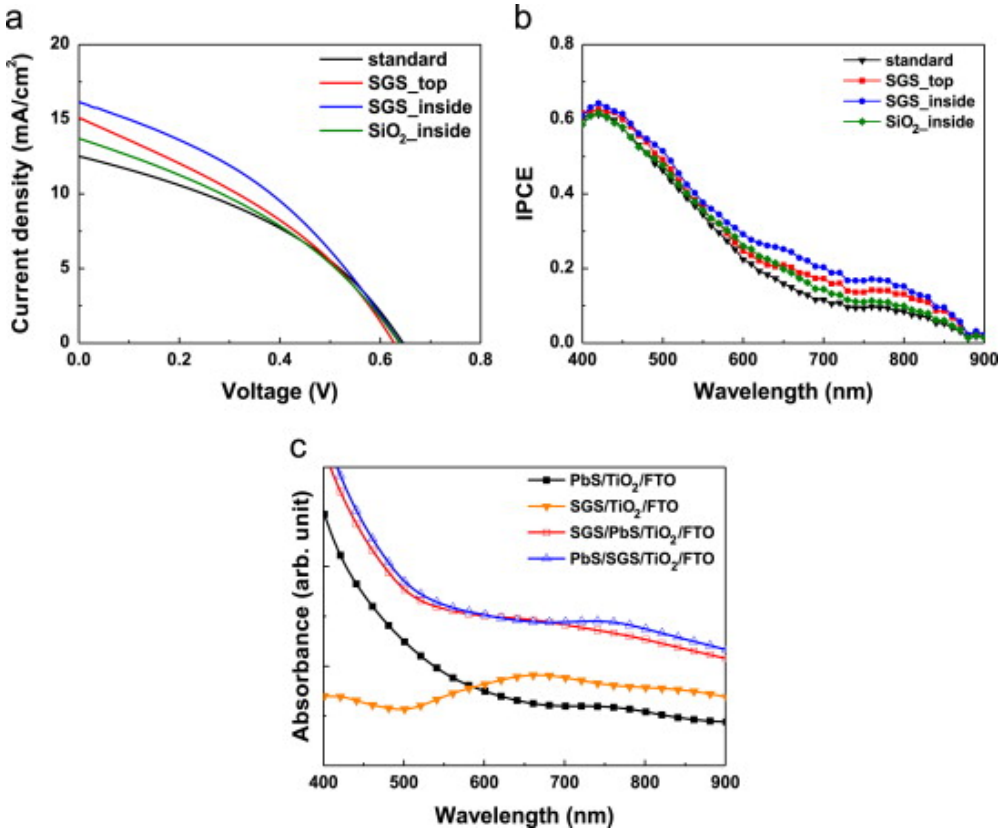


**Figure 11 PbS quantum dot solar cells using plasmonic nanoparticles to increase solar cell performance. the light absorption and IPCE of the cells is greatly increased.[90]**

There are two primary ways that plasmonic particles improve device performance. The first is by increasing light absorption of the solar cell semiconducting layer. The presence of the

electric field increasing the absorption coefficient of the semiconductor film allowing the device to absorb more photons while using the same thickness of material. This allows the solar cell to overcome the traditional tradeoff between light absorption and carrier transport. Since the semiconductor thickness stays the same, the absorbed charges will travel the same distance as a cell with plasmonic nanoparticles so the carrier recombination rate is the same. What is not the same is the light absorption properties of the device. The light absorption for a plasmonic enhanced solar cell is the same as a solar cell with a much thicker semiconducting layer. The absorption spectra of plasmonic nanoparticle can be tuned to absorb light at specific wavelengths. By changing the size and shape of the nanoparticle, the absorption spectra can be shifted to different wavelengths. Traditionally, the larger the nanoparticle the absorption peak shifts to longer wavelengths. [87, 89, 93, 95]

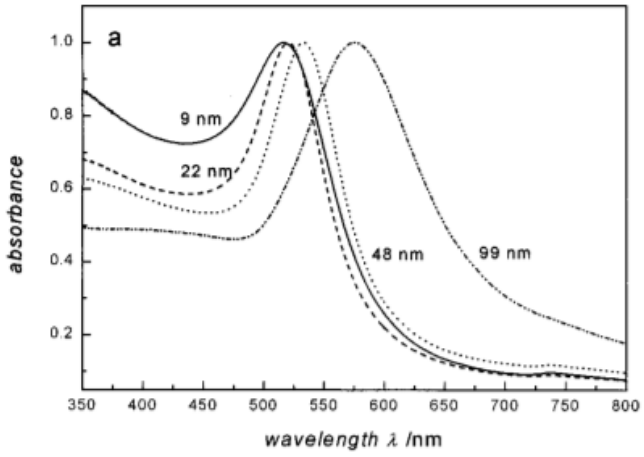


**Figure 12 Plasmonic absorption of gold Nano spheres. Mei scattering equations describe how the size of the metal nanoparticles affects its plasmonic response.**

The increase in gold nanoparticle diameter shifts the absorption spectra to higher wavelength in the experiment shown in figure 12.

There have been many studies to change the nanoparticle shape in the plasmonic response of the plasmonic particles. Efforts have gone into experimenting with cubes, pyramids, spheres, and other irregular shapes affect the device performance of the solar cell.[84, 85, 91]

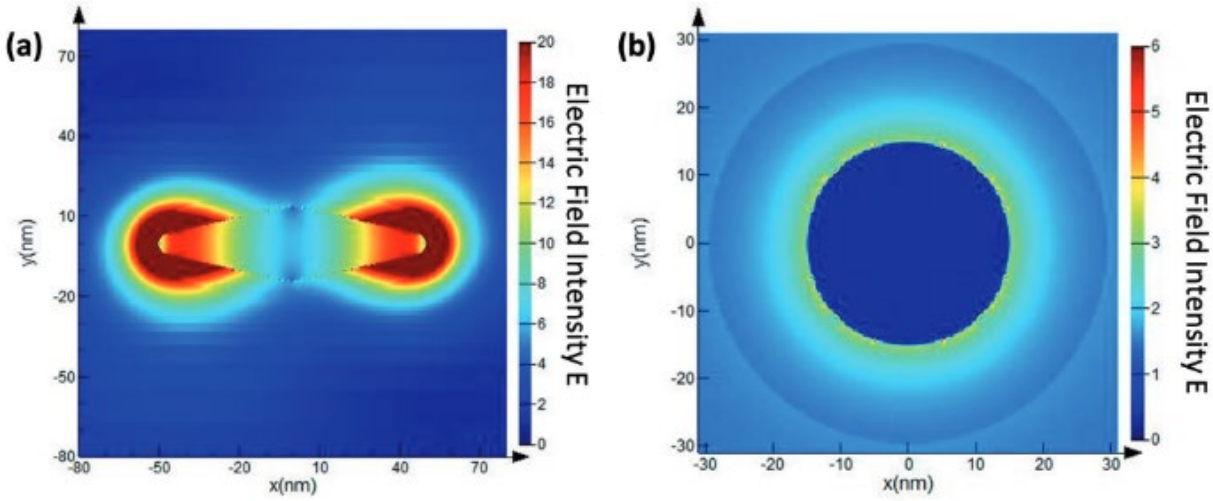


**Figure 13 plasmonic response from a Bipyramidal shaped nanoparticle and a spherically shaped nanoparticle. The Bipyramidal nanoparticle shows a higher plasmonic field intensity**

Shown in figure 11, by using bipyramidal plasmonic nanoparticles, the plasmonic field intensity increases greatly over that of a spherical nanoparticle.[84] The motivation behind this is to use the conical ends of the pyramids to concentrate the plasmonic field. The use of various shapes in plasmonic research has improved the flexibility of engineering variables to control the plasmonic response.

### 1.3.5 Tamm Surface Plasmons

Tamm surface plasmons were first predicted by Igor Tamm, a theoretical physicist, in the 1930's. [101, 102] His work predicted that there are electronic states localized at the surface of crystals due to defects on the crystal surface. i.e. stable electron energy levels in the bandgap of crystals. Tamm surface plasmons are photonic energy levels in the optical bandgap of a photonic crystal. These surface plasmon can be physically created at the interface between a metal and a Bragg mirror. [94, 96, 103-105] A Bragg mirror is made of alternating films of high and low refractive index materials that reflect light though destructive interference. A mathematical analysis of how these plasmon form was described in 2007.

Mathematical explanation: [101]

The proof is in two parts, the first shows that if a certain condition occurs at an interface an electromagnetic stat is formed. The second part shows that the interface between a Bragg mirror and a metal meets those conditions.

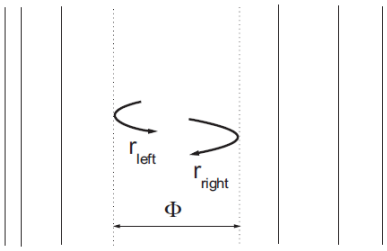


**Figure 14 Two virtual interfaces used to describe the presense of Tamm surface plasmons**

The amplitude of the right reflection coefficient of the left propagating wave $r_{left}$ and the right propagating wave $r_{right}$. Using the transfer matrix method, the equation for the field of the eigenmode is equation 1.

$$A\begin{pmatrix} 1 \\ r_{\text{left}} \end{pmatrix} = \begin{pmatrix} \exp(i\Phi) & 0 \\ 0 & \exp(-i\Phi) \end{pmatrix}\begin{pmatrix} r_{\text{right}} \\ 1 \end{pmatrix} \tag{1.7}$$

A is a constant, iota=nxw/c and is the phase change of the wave. X is the distance between the virtual interfaces, w is the angular frequency, and n is the refractive index.

Eliminating A:

$$r_{\text{left}} r_{\text{right}} \exp(2i\Phi) = 1. \tag{1.8}$$

And reducing x to zero as the two interfaces are joined together:

$$r_{\text{left}} r_{\text{right}} = 1. \tag{1.9}$$

When this condition is met, the eigenmode of the system is met and a possible photonic energy state can form. To show that a Bragg mirror and a metal meet this criteria, the left layer will be a metal and the right material will be the Bragg mirror, $r_m r_{BR}=1$.The amplitude of reflection for a metal is given by the Fresnel equation,

$$r_m=(n_A-n_M)/(n_A+n_M). \tag{1.10}$$

$n_M$ is the refractive index of the metal and $n_A$ is the refractive index of the top dielectric layer of the Bragg mirror. and given by the Drude model as

$$n_M{}^2=\varepsilon_b\left(1-\frac{\omega_p^2}{\omega(\omega+i\gamma)}\right) \tag{1.11}$$

When the frequency is less than the plasma frequency and the collision rate is small,

$$n_M\approx i\sqrt{\varepsilon_b}\frac{\omega_p}{\omega} \tag{1.12}$$

$r_M$ can be approximated by

$$r_M\approx -1-\frac{2in_A\omega}{\sqrt{\varepsilon_b}\omega_p}\approx -\exp\left(\frac{2in_A\omega}{\sqrt{\varepsilon_b}\omega_p}\right)=\exp\left[i\left(\pi+\frac{2n_A\omega}{\sqrt{\varepsilon_b}\omega_p}\right)\right]. \tag{1.13}$$

$R_{BR}$ can be found through the transfer matrix method assuming a large number of layers and w is close to the bragg frequency.

$$r_{BR}=\pm\exp[i\beta(\omega-\omega_0)/\omega_0]\quad \beta=\frac{\pi n_A}{|n_A-n_B|}. \tag{1.14}$$

Therefore, $r_m r_{BR}=1$ becomes

$$\pi+\beta\frac{\omega-\omega_0}{\omega_0}+\pi+\frac{2n_A\omega}{\sqrt{\varepsilon_b}\omega_p}=2\pi l, \tag{1.15}$$

For the solution of when w is close the Bragg frequency.

$$\omega\approx\frac{\omega_0}{(1+2n_A\omega_0/\sqrt{\varepsilon_b}\beta\omega_p)} \tag{1.16}$$

For an interface between gold and a Ga/As/AlAs Bragg reflector with a frequency of 1 eV, equation above predicts a TP frequency of 0.95 eV. The above proof shows that Tamm surface plasmons exist between a metal film and a Bragg mirror and they also occur at the Bragg wavelength of the underlying Bragg mirror. The location of the Tamm surface plasmon can be tuned by adjusting the Bragg wavelength.

The problem comes with engineering a Tamm plasmon using real world materials and how those affect the plasma frequency of a Bragg mirror/metal system.

The geometry of a Bragg mirror and how to control its properties with constituent equation are described in detail in section 1.1-2.

The thickness and type of metal affect the Tamm plasmon system as well. If the metal thickness is too high, no light will be able to reach the metal/Bragg mirror interface and therefore the condition for Tamm surface plasmon resonance will not occur. If the Bragg frequency is higher than the plasma frequency of the metal, the derivation above does not pertain to the system. What will likely happen are photons will broadly be absorbed and no Tamm surface plasmon effect will be observed.

Previous studies have shown that Tamm surface plasmons exist between a Bragg mirror and a thin metal film. [103][106] Most studies have used gold as a metal film however other plasmonic metals such as silver and aluminum are possible. The dielectric materials of the Bragg mirror used are vast. The most common pair found is GaAs and AlGaAs with other common parings being $Ta_2O_5$/ $SiO_2$ and $TiO_2$/$SiO_2$.

### 1.3.6 Bragg Mirrors

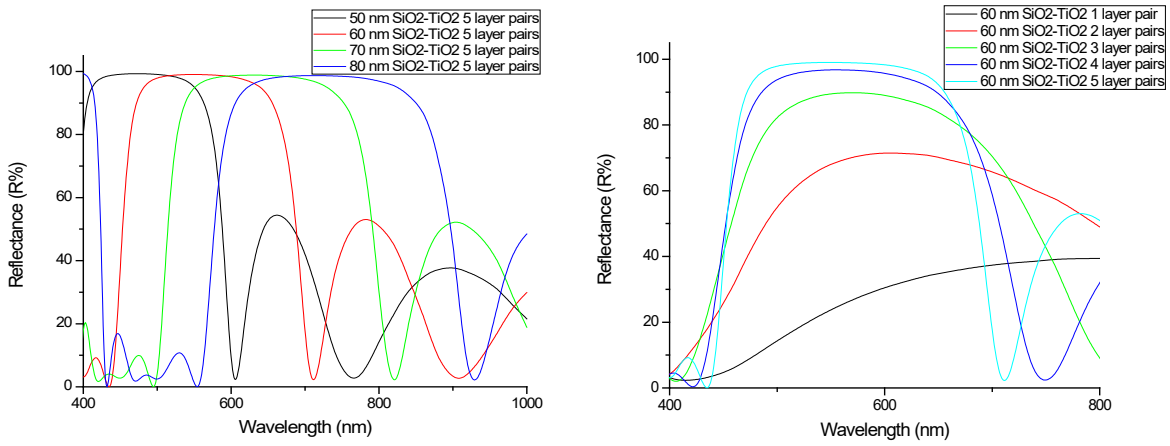


**Figure 15 Simulated Effect of increasing dielectric layer thickness on photonic mirror reflectance peak. (B) Increasing number of dielectric layers and its effect on reflectance**

Photonic crystals are comprised of alternating stacks of high and low refractive index materials. Much like how the spacing and atomic arrangements in semiconductors form a bandgap with forbidden energy levels, the spacing and refractive index difference between dielectric layers prohibits certain wavelengths of light from traveling through the material and forms a photonic band gap. Since the photons are not allowed to be transmitted, they are reflected. The refractive indices and dielectric layer thicknesses can then be controlled to tune the reflected spectrum. The primary metric of the reflectance spectrum is the location of the reflectance peak and width of the reflectance peak. Each of these parameters can be described by the following equations: [107]

$$\lambda_p = 2\left(n_{SiO_2} \times d_{SiO_2} + n_{TiO_2} \times d_{TiO_2}\right) \tag{1.17}$$

$$\frac{\Delta\lambda}{\lambda_p} = \frac{4}{\pi} \times \sin^{-1}\left(\frac{n_{TiO_2} - n_{SiO_2}}{n_{TiO_2} + n_{SiO_2}}\right) \tag{1.18}$$

Equation 5.11 describes how the center reflected wavelength changes based off refractive index and dielectric layer thicknesses. Nh and dh are the refractive index and thickness of the high dielectric constant layer and nh and dh are refractive index and thickness of the low dielectric material. As layer thickness increases as well as refractive index increases, the wavelength of reflected light also shifts to longer wavelengths. The other characteristic of Bragg mirrors is the width of the reflected spectra. Equation 5.12 describes the relationship between refractive indices of the dielectric layers and the reflectance spectra width. As the difference between refractive indices increases between the layer materials, the width of the reflectance spectra also increases. The number of dielectric pairs also impacts the width of the reflectance peak. As the number of pairs increases, the forbidden photon wavelengths in the Bragg mirror become more defined. As more and more layered pairs are formed however, there becomes less and less benefit to depositing more layers. The Tamm surface plasmon mathematical proof assumes there are a near infinite number of dielectric layers defined and broad reflectance spectrum. An optimally engineered Bragg mirror will be highly reflective and have a highly and a under defined reflectance spectrum will not satisfy the mathematical conditions laid out in previous sections. The dielectric materials must also be transparent to visible and near infrared photons. Many materials have high dielectric constants in the visible range but they also have small band gaps which allows for photon absorption by the semiconductor. Because of this, common high and low dielectric materials used in Bragg mirrors are $TiO_2$ and $SiO_2$ respectively. Their refractive indices are 1.5 and 2.5 respectively.[108, 109] These materials are commonly used in Bragg mirrors as their fabrication methods and parameters have been heavily studied.

### 1.3.7 Nanoscale fabrication methods overview

#### 1.3.7.1 Spin Coating

Spin coating is a simple nanoscale deposition technique to form solid uniform films from solutions. During a typical deposition step, small monomers of the film are dissolved in a solvent that readily evaporated. The solvent is coated on a flat substrate and the substrate is spun at hundreds to thousands of rpm. [110, 111]

As the substrate spins, the solution is evenly distributed across it. As the spinning continues, the solvent evaporates leaving the dissolved solids behind. The thickness of the film can be controlled by adjusting the concentration of the solution and it is inversely proportional to the square the the spinning speed. By increasing the spinning speed by 4, the film thickness will decrease by half. The crystallinity or other parameters of the film can be controlled by post treatment such as high temperature annealing steps to increase crystallinity.

#### 1.3.7.2 Sputtering

For sputtering, the general description of the deposition process is as follows. An ionized gas, usually argon, is accelerated into a target material at high velocity. The argon hits the target breaking interatomic bonds to dislodge atoms. The material is ejected from the target and coated on the substrate. The process is done under a vacuum to maintain a high purity environment and so the barrier for material transport is low between the target and the substrate. [112-118]

For reactive sputtering, the principles are the same however a reactive gas, in this case oxygen, is introduced into the sputtering gas. The sputtering gas will dislodge and also react with the sputtering target material to form an oxide.

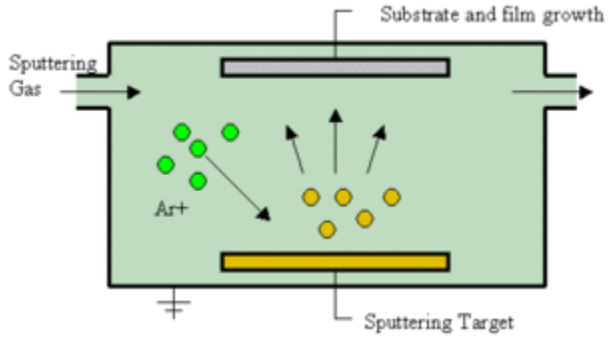


**Figure 16 Sputtering diagram high velocity argon hits the sputtering target dislodging material. The material coats the substrate to achieve film growth.**

The following variables can be altered to affect the deposition rate

Sputtering power: higher power increases the number/speed of argon atoms hitting the substrate. A higher power will increase the deposition rate. Too high of a power may crack/ damage the sputtering target.

Voltage: this is the bias voltage between the argon ions and the sputtering target. A higher voltage at a constant power will decrease the number of argon ions striking the target but the argon ions will have a higher kinetic energy and momentum. A higher voltage is useful to sputter targets with stronger inter atomic bonding/ heavier atoms.

Processing pressure: at a low processing pressure, there will not be enough argon atoms to hit the sputtering target resulting in inefficient deposition. If the processing pressure is too high, the excess gas in the chamber will interfere with the motion of the sputtered target atoms to the substrate. For this condition, the sputtered material will coat the whole inside of the chamber instead of just the substrate resulting in wasted material and low deposition rate. There is an optimized processing pressure for each material and processing power. This optimized range is usually between 3 and 15 mTorr.

Substrate temperature: This variable can determine the overall crystallinity/ overall density of fabricated films. If you are planning on making a device at an elevated temperature, do the rate run at an elevated temperature.

Base pressure: This is a crucial deposition parameter that is important to control to maintain consistency between runs.

#### 1.3.7.3 Electron beam evaporation

Electron Beam evaporation is a relatively simple deposition method that excels at depositing thin metallic layers along with some oxide materials. Under vacuum, a target source is bombarded by an electron beam that heats the source material. The source material will form a liquid and eventually evaporate or sublimate at a high enough temperature. The evaporated material is transported to the substrate under vacuum and evenly coats it. The substrate can be at room temperature or heated depending on final properties required for the film.

Oxides can also be deposited but due to high temperatures and vacuum environment, the resultant film will be oxygen deficient. [119-121]

#### 1.3.7.4 Atomic layer deposition

The primary use for atomic layer deposition is to deposit thin, uniform, and defect free films with high control over the films properties. ALD is a subset of chemical vapor deposition that uses gaseous precursors in sequence to build up a film. traditional chemical vapor deposition grows films in a steady state manor with all precursors being introduced in the deposition chamber at the same time. The growth of films through ALD occurs in a step wise manner.[122-127] In a prototypical deposition cycle, two precursors are used, A and B. Precursor A is introduced into the reaction chamber and is physisorbed onto all reachable surfaces in the chamber, e.g. the reaction

walls the substrate in which the film needs to be deposited on. Since the number of reaction site in the chamber and on the substrate is finite, excess precursor A remains in the chamber and is eventually removed from due to the vacuum. Precursor B is introduced which reacts with the physisorbed A precursor to form the final required film. The reactants and bi-products for film growth are removed from the chamber by the vacuum. This cycles creates one layer of film and can be repeated for additional film growth. For the formation of $TiO_2$ films, Tetrakis(dimethylamido)titanium or TDMA-Ti is commonly used as a precursor A and a strong oxidant is used as precursor B to get an oxide film depending on the type of ald process used.

Three main ald processes that can be used are thermal, ozone, and plasma ald. Each of these types vary depending on the strength of the oxidizer being used. Typically, thermal ald uses water as a oxidizer and the operating temperature of the deposition process ranges from 150 to 350 °C. ozone and plasma ald have stronger oxidizing precursors with O3 and oxygen plasma so a high temperature is not required for complete reaction of the precursors leading to higher purity films made at much lower temperatures. Plasma ALD allows for nitrides and metals to be deposited by reacting precursor A with Nitrogen or Hydrogen plasma. [128-131] Using strong oxidants like ozone or oxygen plasma are incompatible with thin metal films that are prone to oxidation because the metal film will oxidize completely.

#### 1.3.7.5 Cleaning methods and operational procedures.

For the fabrication of nanoscale devices, small micrometer size contaminants such as dust, hair, or oils will cause great damage to the device. For this reason, substrate cleaning and handling is of the utmost importance. Substrates were mostly handling in a class 1000 clean room and washed with acetone/isopropanol sonication methods before additional layers were made.

## 2.0 Motivation

**1.** For use in solar cell devices, as fabricated quantum dots will make quantum dot films have very low carrier mobility, and overall, poor charge transport behavior. The reason behind this is the long oleate ligands on the surface of the quantum dot. The oleate ligands are necessary for stabilizing the surface of the quantum dot as well as dispersion in solvents but, the ligands have long organic chains that greatly increase the quantum dot particles spacing increasing the barriers for change transport.

**2.** The pros of using EDT as a ligand is it promotes charge transport within the film. The EDT ligand while it is small, ligands could theoretically be smaller as the EDT ligand is comprised of 10 atom. Also, for more complicated devices, the rigidity of only using P type materials in solar cells will greatly limit future solar cell designs. Having the option to use an N type PbS materials would open up new device architectures that can improved solar cell performance than just using P type PbS on its own.

**3.** Using solid state ligand exchange techniques does not completely remove the native oleate ligands on the quantum dot surface. this means there are 1. Unpassivated lead sites on the quantum dot surface that act as recombination centers 2. Long chain oleate ligands increase the overall particle spacing. Both of these factors reduce the charge transport behavior in quantum dot films.

**4.** while the improvement of PbS solar cell efficiency has been remarkable using iodine ligands and improved ligand exchange techniques, the efficiency is still uncompetitive to be used as a commercial power generation device. Research in ligand exchange for PbS has essentially reached a limit as devices are being fabricated with the smallest possible ligand to reduce electron

hopping distances. The quantum dots surface has been confirmed to be entirely terminated with iodine ligands through a combination of solid and liquid exchange techniques. For PbS quantum dot solar cells to advance, different strategies must be pursued.

**5.** due to the limited energy transitions around the band gap energy due to discrete energy states, light absorption is poor in PbS quantum dots in the near infrared range. Simply increasing film thickness does not increase the light absorption properties in the NIR range significantly. The increase film thickness negatively impacts recombination in the cell while not improving light absorption. For visible light, the absorption coefficient for PbS is already high, so increasing film thickness is redundant. The biggest improvement for PbS solar cells would be to increase the light absorbance in the quantum dot film for just the NIR region.

**6.** One issue with using pure metal nanoparticles is there is a direct contact between the semiconductor absorber and the metal nanoparticle. The presence of this metal dielectric film has shown to create mid-gap states in the semiconductor and it acts as recombination centers which decrease charge transport behavior in the solar cell.

One way researchers have overcome this phenomenon has been to add a dielectric shell to the nanoparticle. The addition of the dielectric shell reduces the recombination rate in the solar cell while still providing surface plasmon resonance fields. The dielectric shell increases the size of the nanoparticle allowing for more light scattering to occur. As light in scattered in the semiconductor absorbing layer, the light's optical travel path increases in the semiconducting film increasing its effective film thickness as light can travel father in the film. Since the metal is covered with an inert dielectric layer, there is less of an opportunity for degradation of the metal film through attacks from environmental oxygen or water.

**7.** core shell nanoparticles are versatile and stable there is a limit design range for these nanoparticles. With only the size of the nanoparticle being controlled, the plasmonic range of plasmonic response is low. By controlling the nanoparticle shape, more variables can be controlled and the plasmonic response can be controlled more effectively.

**8.** The approach of using nanoparticles as the plasmonic source is fundamentally flawed however. All nanoparticle approaches suffer from the same flaw in that the area of absorber material in the solar cell affected by the plasmonic effect from the nanoparticles is very small compared to the absorber area. This is due to the fact that the coverage of the nanoparticles is limited.

**9.** To find mobility and other charge transport metrics from a solar cell is not straightforward. There are two different charges that are transported in a PbS film, both holes and electrons and are both equally important in solar cell performance. If either of the hole or electron charges recombine, that is energy lost to heat. When quantifying PbS solar cell performance through the opto-electronic methods, it is important to understand the physics of charge transport. For a traditional PbS quantum dot, the cross section of a device is shown in figure 12. There is a transparent conductor, FTO, mesoporous $TiO_2$ electron transport layer, PbS film, $MoO_3$ hole transport layer, and a thick gold film.

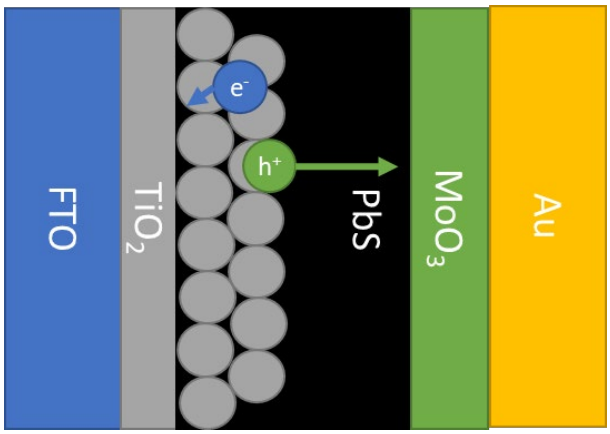


**Figure 17 Cross section of a traditional quantum dot solar cell structure.**

For this structure, electrons and holes are generated in the PbS layer. Electrons travel to the $TiO_2$ layer and holes travel to the $MoO_3$/gold layer for extraction. The opposite travel direction of positive and negative charges produces a net current. Most holes and electrons are generated near the $TiO_2$/PbS interface as the light intensity decays exponentially into the PbS film. From this, electrons must travel a short distance in the PbS film compared to the generated holes. Therefore, hole transport is more important than electron transport in this device based on its architecture. Additionally, due to the mesoporous layer that is normally around a micrometer, there is a large portion of charge transport that occurs in other layers besides the PbS. This complicates finding diffusion and mobility coefficients for the device. Since the device is only stimulated in one direction, only the transport properties of one charge carrier is really being measured.

# 3.0 **Hypothesis**

1. Dual illumination provides a tool for characterizing carrier transport of minority and majority carriers in quantum dot solar cells using. By creating two illumination directions, hole and electron transport mechanics can be separately determined.

2. Plasmonics will reduce the tradeoff between charge transport and light absorption in PbS quantum dot solar cells. Plasmonic thin films increase the light absorption in PbS while keeping the PbS film thickness the same and therefore, keeping the charge transport properties the same. The plasmonic thin film can be tuned to match poor light absorbance regions in PbS films to increase carrier collection and extracted current.

# 4.0 PbS Dual Illumination Characterization

## 4.1 Experimental background

Measuring hole and electron transport in quantum dot films is not a straightforward endeavor. Both hole and electron mobilities can be measured by Hall effect measurements or through field effect transistors. Hall effect measurements may not be feasible to measure charge kinetics in quantum dot films as the conductivity of PbS is very low and will require expensive high precision voltage/current measurement equipment along with a strong enough magnetic field. Transistors can be difficult to fabricate as they require some microfabrication techniques. Even if values from these measurements can be found, the conditions the PbS film is measured in do not match the operating conditions in a solar cell device and may have little physical significance. For example, mobility measurements from a transistor can find kinetics of both holes and electrons however the device is unipolar, meaning only one charge carrier is present at a time. [132]This is in stark contrast to real solar cell operation where holes and electrons are present in the device at the same time. In fact, the recombination probability, and therefore transport properties, are proportional to the concentration of opposite charges. E.g. the recombination probability of electrons increases as the concentration of holes also increases. Shown in table 1 are diffusivities and mobilities of holes and electrons measured through transistors and hall effect measurements.

**Table 1 Electron and Hole Mobility in PbS quantum dot solar cells using transistors, hall effect measurement systems, and Current decay measurements [40, 61, 72, 78, 133-141]**

| Measurement Type | Film | Electron Mobility ($cm^2/Vs$) | Hole Mobility ($cm^2/Vs$) |
|---|---|---|---|
| Transistor | PbS_MPA | 5.00E-02 | 6.00E-03 |
| | PbS_MPA | 2.00E-01 | 8.00E-04 |
| | PbS_MPA | 1.40E-02 | 3.00E-03 |
| | PbS_BDT | 1.80E-05 | 3.80E-05 |
| | PbS_EDT | 1.70E-03 | 2.30E-04 |
| | PbS_EDT | 8.00E-03 | 1.00E-03 |
| | PbS_TBAI | 6.00E-02 | - |
| | PbS_TBAI | 1.90E-02 | 1.50E-03 |
| | PbS_Bulk | 6.00E+02 | 7.00E+02 |
| Hall Effect | PbS_TBAI | n/a | n/a |
| Current decay | PbS_EDT | 7.20E-04 | n/a |

To find the kinetics of hole or electron transport in solar cell devices, transient current decay measurements must be used and based off the decay curves and the geometry of the solar cell measurement. Traditionally, the geometry of the solar cell will only determine the kinetics of one carrier, the carrier that has to travel the longest. The current decay measurement will be the result of the charge carrier that takes the longest time to be extracted from the solar cell. i.e. the carrier that has to travel the farthest distance. The carrier that must travel the farthest distance is

limited by the geometry of the device and how the intensity of light decays exponentially in a semiconductor film and a solar cell usually can only be illuminated from one direction.

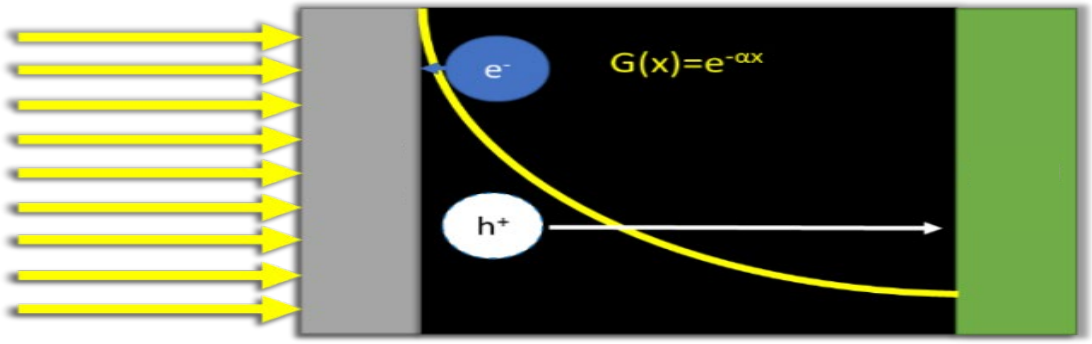


**Figure 18 Generalized solar cell with a transparent electrode in grey, the black absorbing active layer, and the green metal back contact. The generation rate decay exponentially as the light intensity also decreases exponentially.**

In figure 18, the transparent electrode collects electrons and the metallic film collects holes, in this solar cell geometry, holes have to travel farther and are therefore the limiting factor in the current decay measurement. For this solar cell, the kinetics of the hole can only be measured as shining light through the metal back contact will not generate any current as it is reflected.

## 4.2 Experimental set up

Our experimental design is to use two illumination directions to measure the kinetics of both holes and electrons by fabricating the solar cells with two transparent electrodes shown in figure 19.

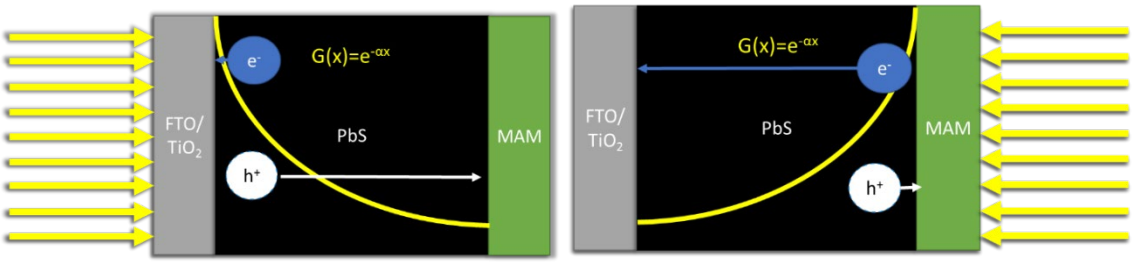


**Figure 19 Dual illumination experimental set up. By changing illumination directions, the carrier that takes the longest to be extracted can be changed.**

In this schematic, when light is illuminated through the FTO side, the charge generation rate decreases exponentially as the distance from the FTO film increases. Therefore, generated electrons much travel a very short distance compared to the holes making the device hole transport limited. When the device is illuminated through the MAM illumination direction, electrons must travel farther than holes so the device performance is electron transport limited.

Simply by switching the illumination directions, hole and electron transport can be qualitatively measured while the device is under normal solar cell conditions.

### 4.2.1 PbS quantum dot fabrication

PbS quantum dots can be fabricated uniformly and constantly through a synthesis method pioneered by Hines and Scholes. The detailed mechanism Is described in the state of the art section and a detailed synthesis route for our specific quantum dots is detailed below.

PbS quantum dots with an absorption peak at 900 nm were fabricated by an adjusted recipe pioneered by Hines and Scholes. Prior to synthesis ODE was degassed under vacuum at 85 °C for 12 hours. 450 mg of PbO, 18 ml of ODE, and 1.5 ml of OA were mixed in a three neck flask under vacuum at 70 °C for 3 hours. Under air free Scheck line conditions, the atmosphere of the flask was switched to nitrogen and the temperature was raised to 95 °C for an additional hour or until the mixture became clear. A syringe of 10 ml of ODE and 207 uL of TMS was prepared as the temperature of the flask was raised to 115 °C. The flask was removed from an oil bath while the temperature of the solution was monitored with an in-situ thermal couple. To initiate PbS formation, the syringe of ODE and TMS was swiftly injected into the PbO-Oleate mixture. What follows is the sudden drop in temperature and the nucleation of black PbS quantum dots. The solution cooled naturally to room temperature under nitrogen flow prior to purification. To form quantum dots with 800 and 1000 nm absorption peaks, 1.25 and 2 ml of oleic acid were used in the lead oleate solution. The quantum dots were separated from the reaction solution by mixing with acetone and centrifuging. This solution was then dispersed in hexane and stored in a low humidity desiccator. Prior to PbS film deposition, the PbS solution was further purified by centrifuging the quantum dots in a mixture of acetone and methanol and drying over nitrogen. This process was repeated three times before the PbS was dispersed in hexane at a concentration of 25mg/ml.

### 4.2.2 Solar Cell fabrication

Tec 15 FTO was used as a transparent conductive bottom contact for all samples. Prior to use, the FTO was patterned by selectively removing FTO through wet etching with zinc powder and 18% HCl in water for 30 seconds. Patterned FTO substrates were cleaned through sequential sonication under Acetone, DI water, and Ethanol for 20 minutes each. Substrates were dried under compressed air and treated for 20 minutes under a deep UV/Ozone treatment for 10 minutes.

A 20 nm $TiO_2$ layer was then deposited on the patterned FTO substrates through ozone assisted ALD between TDMA-Ti and O3 at precursors at 250 °C in a Nanotech Savannah ALD.

To form PpS quantum dot films, spin coating was performed in a low humidity, nitrogen filled glove box. For a spin coating cycle, the fabricated plasmonic substrates were spun at 2500 rpm. 40 ul of PbS in hexane was spin cast on the surface of the substrate, 80 ul of 2 V/V% of EDT in acetonitrile was used to exchange the native oleate ligands with short thiols, finally, 80 ul of Acetonitrile was cast on the spinning substrate to clean the film. N type PbS films were made through similar methods. 40 ul of PbS in hexane was spin cast on the surface of the substrate, 80 ul of 10mg/ml of TBAI in methanol was used to exchange the native oleate ligands with iodine, finally, 80 ul of Acetonitrile was cast on the spinning substrate to clean the film. Each Spin coating cycle deposited 20 nm of PbS and can be repeated to build up a thick film.

The top contact was deposited through ebeam evaporation. 10 nm of $MoO_3$, 10 nm of Au, and 10 nm of $MoO_3$ were deposited in series to form a dielectric-metal-dielectric conductive/transparent contact.

The solar cell active area was 0.0375 $cm^2$ (1.5x2.5 mm) which was controlled by the overlap of the bottom gold film and the top MAuM layer.

### 4.2.3 Solar Cell Characterization

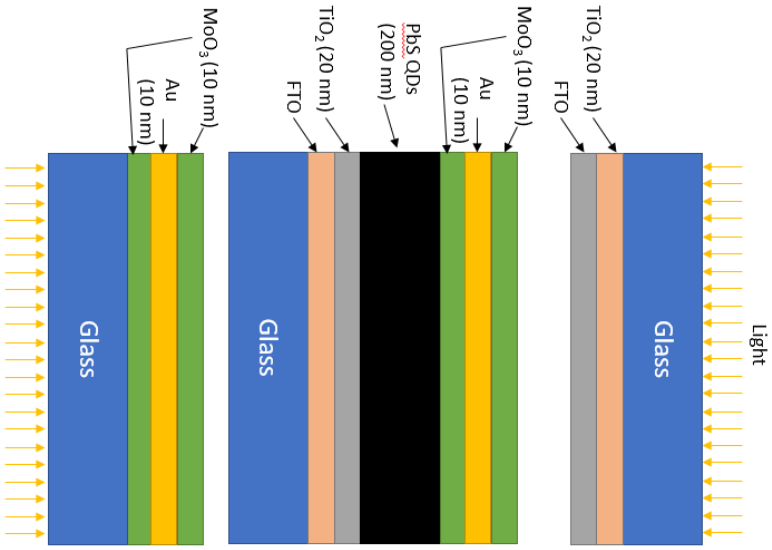


**Figure 20 Set up of optical illumination measurements. Before striking the PbS quantum dot film. The light will be filtered by illumination from FTO and MAM films.**

To determine the kinetics of both holes and electrons, a dual illumination technique is shown in figure 20. The reason why light is passed through filters before striking the solar cell for both illumination directions is due to the necessity of keeping the light intensity the same for both each test. If the light intensity is not the same, quantitative comparisons cannot be done as the extracted current will be affected by differences in charge transport and generation instead of just charge transport.

Voltage and current kinetic decay measurements were done using the SLIM method as described in previous reports. Monochromatic laser beam with an instant turning off at a steady state is generated from a laser diode (λ=445 nm) which is controlled by a function generator (Agilent 33220A). A voltage decay from the steady state is monitored by an oscilloscope

(Tektronix, TDS2024B) that is synchronized with the function generator. The set up for current decay is similar with a current amplifier connected between the sample and the oscilloscope. Decay constants were found by fitting the resultant decay curves to the function: y=e^(-at). The decay constant, a, obtained from the voltage decay measurement is the average charge carrier lifetime. The decay constant obtained from the current decay measurements can be converted to charge diffusion coefficient D=(L^2)/(2.37*a) where L is the thickness of the PbS layer. The mobility can then be found from the Einstein kinetics equation: [142]

$$D = \frac{\mu_q \, k_B T}{q} \tag{4.1}$$

where D is the diffusivity, u is the mobility, k is Boltzmann's constant, T is the temperature, and q is the charge of one electron.

## 4.3 Results

### 4.3.1 Pure P and N type PbS

The first experiment done was to determine the kinetics of holes and electrons in P and N type PbS. Solar cells with structures shown in figure 21 were fabricated using the procedures described in the previous section.

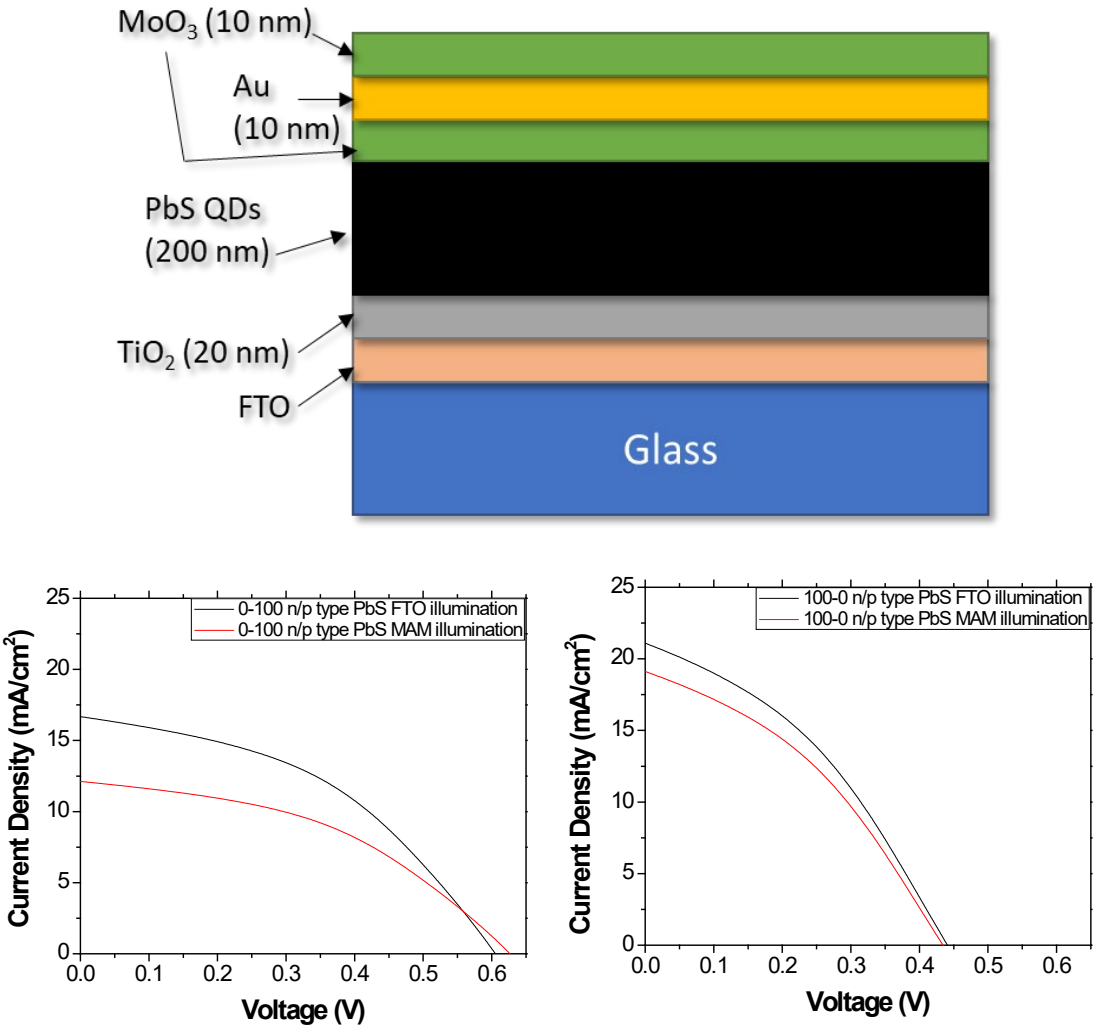


**Figure 21 Cross section of the fabricated solar cells. JV measurements of PbS cells with P and N type ligands under the dual illumination scheme.**

**Table 2 Table showing the qualitative metrics of fabricated P and N type PbS solar cells in figure 17:**

| PbS Cell | Jsc (mA/ $cm^2$) | Voc (V) | N (%) | FF |
|---|---|---|---|---|
| 0-100 n/p-FTO ill. | 16.678 | 0.606 | 4.345 | 0.430 |
| 0-100 n/p-MAM ill. | 12.118 | 0.626 | 3.281 | 0.432 |
| 100-0 n/p-FTO ill. | 21.096 | 0.441 | 3.465 | 0.372 |
| 100-0 n/p-MAM ill. | 19.119 | 0.434 | 3.095 | 0.373 |

The EDT and TBAI ligands impart iodine and sulfur onto the surface of PbS. The addition of a iodine from TBAI onto the surface of the PbS generates a free electron for charge compensation imparting n type behavior into the semiconductor. The addition of sulfur from the thiol group in EDT generates a hole from charge compensation imparting P type behavior. the differences in which ligand is used to passivate the surface can greatly change the electrical properties of the quantum dot film as well as the device the film is used is.

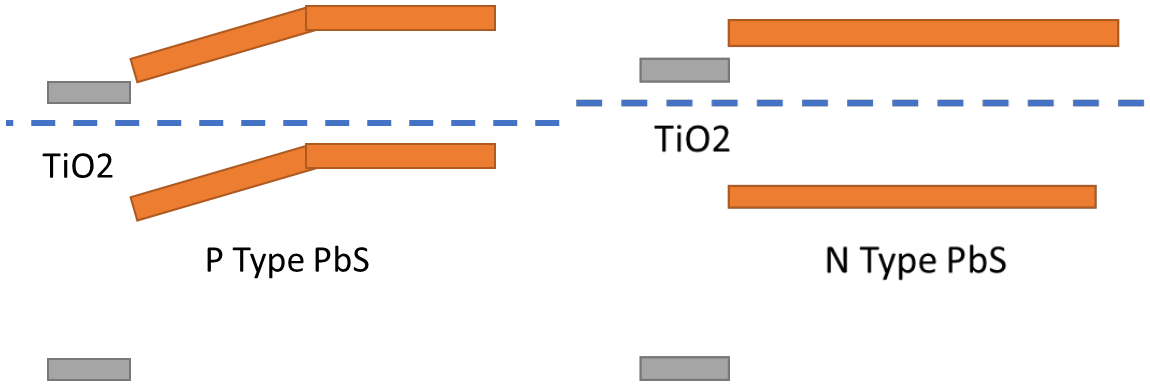


**Figure 22 Band Diagrams of P and N type PbS solar cells with $TiO_2$.**

Shown in figure 21 are the current density/ voltage measurements of n and p type PbS solar cells illuminated using the dual illumination technique. Shown in table 1 are the metrics to describe the current density/voltage curves. Between N and P type PbS solar cells, N type PbS devices have a higher current density at 21 mA/ $cm^2$ for fto illumination versus, 16.67 mA/ $cm^2$ for P type devices. The open circuit voltage of the device is 0.6 V for P type PbS and 0.44 for N type PbS.

Between illumination directions, N type PbS retains 90% of extracted current when the illumination direction is switch from FTO to MAM illumination. P type PbS solar cells only retains 73% of its extracted current when the illumination direction is changed from FTO to MAM illumination.

To determine why there is a large change in extracted current for P type PbS and not N type PbS devices from FTO to MAM illumination, even though the illumination intensity is the same the kinetics, of both holes and electrons need to be measured.

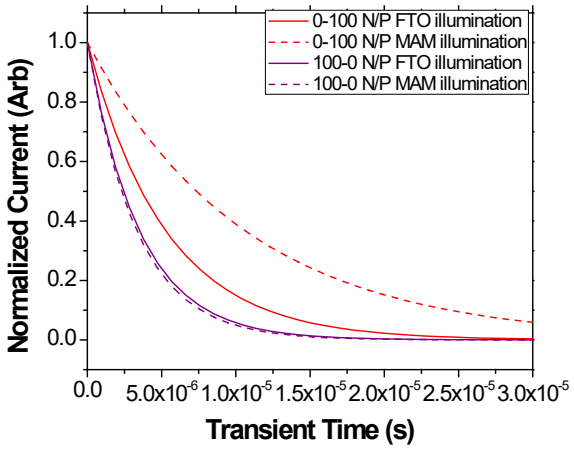


| PbS Type | Carrier | Transient Time | Diffusion Coefficient (cm2/s) | Mobility (cm2/(V·s)) | Lifetime (us) | Diffusion length (nm) |
|---|---|---|---|---|---|---|
| N type | Hole | 3.50E-06 | 4.82E-05 | 1.87E-03 | 1.05E+02 | 291.87 |
| N type | Electron | 3.32E-06 | 5.08E-05 | 1.97E-03 | 1.05E+02 | 299.67 |
| P type | Hole | 5.27E-06 | 3.21E-05 | 1.24E-03 | 1.17E+02 | 251.17 |
| P type | Electron | 1.06E-05 | 1.59E-05 | 6.17E-04 | 1.17E+02 | 177.04 |

**Figure 23 Current transient measurements taken from a SLIM-PC decay method. Calculated diffusion, mobility, lifetime, and diffusion length for holes and electrons in P and N type PbS using the dual illumination current decay technique.**

Figure 23 shows the transient current decay measurements for all P and N type devices for both FTO and MAM illumination. The transient times for FTO and MAM illumination directions are nearly identical for the all N type PbS device. The all p type device however show that when

illuminated from the MAM side, it takes much longer for the device to reach equilibrium owing to slower kinetics from light directed at the MAM side.

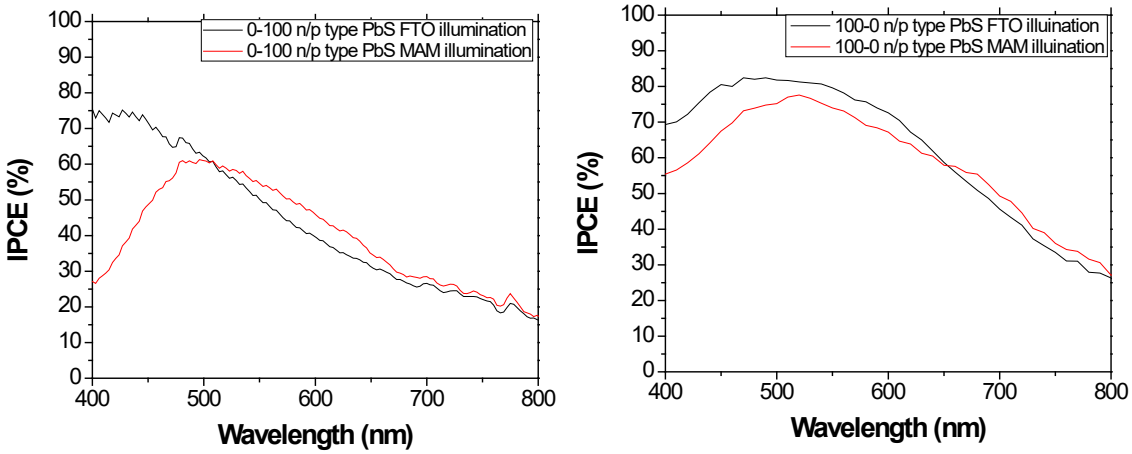


**Figure 24 IPCE measurement of all p type and all n type PbS quantum dot film active layers illuminated from the MAM and FTO directions**

The IPCE in figure 24 shows a similar trend as what was found in the IV and transient decay measurements. For the P type PbS cell, there is a large difference in quantum efficiency for short wavelength photons. The IPCE for 400 nm photons is 75 for FTO illumination and 25 for MAM illumination. The N type solar cells show minor variations in IPCE and the overall shape of the curve is the same.

To explain the difference in extracted current and open circuit voltage, the band diagram shown in figure 22 is consulted. Due to the differences in fermi energy levels between n and p type PbS, the band bending when $TiO_2$ and $MoO_3$ are in contact with the films also changes as the fermi energy across the device must be at equilibrium so no net charge flow will occur. From the P type PbS diagram, the difference in fermi energy levels between the N type $TiO_2$ and P type PbS is quite large. The consequence is there will be a large amount of band bending and the voltage

needed to overcome the difference in fermi level will be large. This leads to a high open circuit voltage for the P type device. The open circuit voltage is lower for N type PbS because the fermi levels between N-type $TiO_2$ and N type PbS are closer, and as much band bending will not occur.

For both cells, there is slight band banding at the $TiO_2$/PbS and PbS/ $MoO_3$ interface. For the band bending regimes, main charge transport mechanism is drift as the energy where the energy level bending pushes holes and electrons up or down an energy gradient.

The difference between FTO and MAM illumination is due to changing how far electrons and holes must travel to escape from the PbS cell and to the much more conductive metallic electrodes. For FTO illumination, the majority of charges are generated close to the $TiO_2$/PbS interface as light intensity and therefore charge generation, decays exponentially. The result from this is electrons must travel a short distance to the FTO layer whereas holes must travel farther to the MAM electrode. In terms of consequences for device performance, when illuminated through the FTO side, hole transport kinetics become the limiting factor to efficient charge extraction. For MAM illumination, the exact opposite occurs; electrons must travel further than holes and electron transport becoming the limiting factor for the solar cell performance.

This give preliminary qualitative information to explain why illuminating P type PbS in the MAM illumination direction extracts much less current than through the FTO illumination scheme. Electron transport in P type PbS is worse than hole transport. To qualitatively study the just how holes and electrons travel in N and P type PbS, current transient measurements were done using the SLIM-PCD method. This technique uses a monochromatic laser diode to excite charges in the solar cell device. The lasers intensity is then reduced very quickly. Since the light intensity has decreases, the extracted current will also decrease. This method records the rate of decay of current as charges must be extracted to reach a new equilibrium. Again, the dual illumination

principle will be used so the kinetics of hole and electron transport can be measured by simply changing the illumination direction. If the measured current decays quickly, the system has reached equilibrium faster and therefor, charges have been transported out of the cell faster.

The reason for the higher current in N type devices can be explained by the transient curves in figure 21, both holes and electrons travel faster in N type PbS than P type PbS as the device reaches equilibrium faster. The next natural question is why is there a significant difference in hole and electron transport in P type PbS and not N type PbS. This might be explained by the effective mass differences between holes and electrons in P type PbS. However further simulations may be required to prove that hypothesis.

### 4.3.2 Effect of quantum dot size on Charge Transport

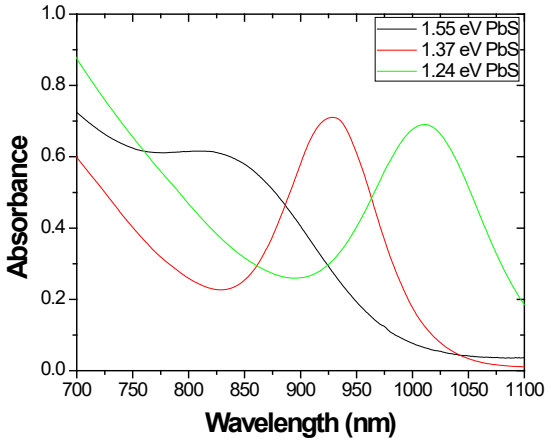


**Figure 25 Absorption spectra of different diameter PbS quantum dots**

Figure 25 shows the quantum dot absorption peaks of 1.55, 1.37, and 1.24 eV PbS quantum dots. Using tabulated size data to match the bandgap of the quantum dot to its diameter. The sizes

of the fabricated quantum dots are 2.75, 3.15, and 3.5 nm. As the size of the quantum dots get smaller, the band gap increases and a blue shift occurs for the absorbance peak position.

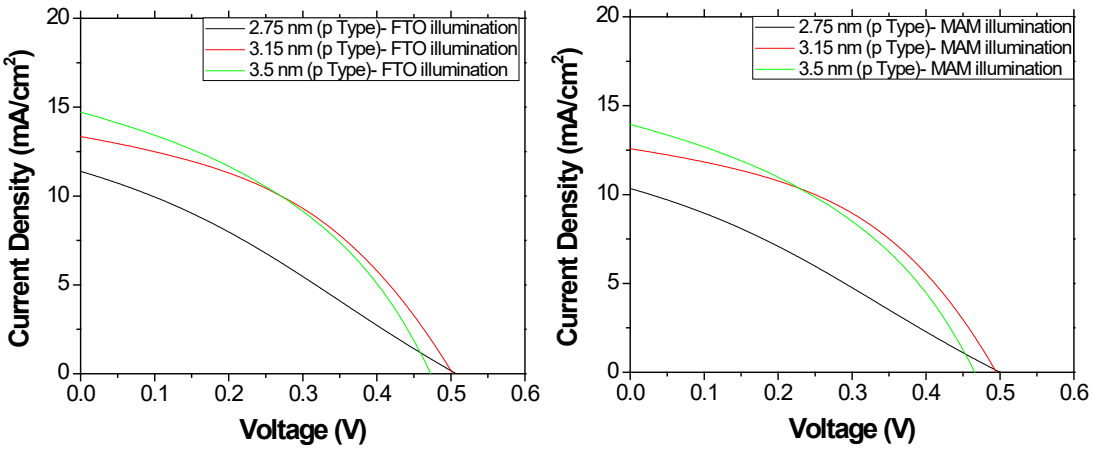


**Figure 26 JV curves of P and N type PbS quantum dot solar cells with different sized quantum dots**

Figure 26 shows the IV curve results of PbS solar cells fabricated with three different sized quantum dots shown in figure 26. Three main trends occur, the first is that as the size of the quantum dot increases, the short circuit current increases and the open circuit voltage decreases. The decrease in open circuit voltage is due to the decrease in bandgap of the quantum dot film as size increases. The decrease in the bandgap reduces the built in potential of the cell. There are two possible reasons for an increase in extracted current as the particles get larger, the first is an increase in light absorption. As the band gap decreases, higher wavelength, lower energy photons can be absorbed and more electrons are generated. The second is an increase in the charge carrier transport of the PbS films. As the PbS quantum dots increase in size, there will be less PbS-PbS interfaces that can be potential recombination sites. Fewer recombination allow for higher mobility

of charge carriers and therefore a higher extracted current. To elucidate this, more characterization was done.

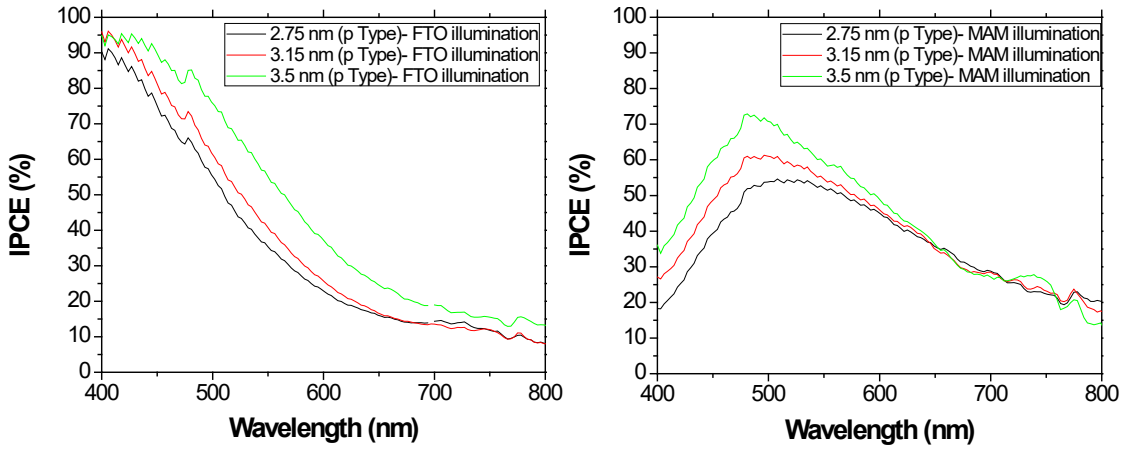


**Figure 27 IPCE data for solar cells illuminated through front and back illumination using different ized quantum dots ans absorbing layers**

To analyze the IPCE data in figure 27, the data must be looked through two different facts in mind. The first is that by switching illumination direction, the distances traveled for holes and electrons are switched. For illumination through the FTO side, holes travel farther than electrons so the device is hole mobility limited. For illumination through the MAM side, electrons travel farther than holes so the device is electron mobility limited. This is especially true for high energy photons, low wavelengths, as they are absorbed very shallowly to the PbS layer so the relative distance effect is amplified.

In figure 3 between 400 and 500 nm, the device under FTO illumination shows very high IPCE around 90%, the same device however when illuminated under MAM illumination shows a drastic decrease in its IPCE down to 40%. This gives evidence that hole transport in PbS quantum dots much better than electron transport. Most of the electrons that are generated far away from

the $TiO_2$ junction do not contribute to the current in the device. This is further seen in the IV curves of front and back illumination of the solar cell devices.

For smaller quantum dots, the carrier transport for both holes and electrons decreases as the size of the quantum dots decreases. To confirm that the decrease in IPCE is due to a decrease in carrier transport, current decay measurements were done to determine the kinetics in the PbS film.

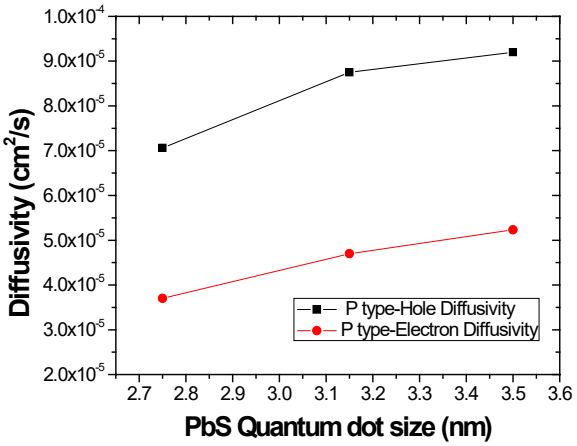


**Figure 28 diffusivity coefficients for both holes and electrons in PbS quantum dot films with variously sized quantum dots.**

Shown in figure 28, the electron and hole kinetics slowdown in PbS films as the quantum dot size increases. This matches the previous data showing that small PbS quantum dots may have charge transport problems. The diffusivity for holes and electrons for a 2.75 nm diameter quantum dot is 30% less than that of a 3.5 nm quantum dot. This can explain why the extracted current density for PbS quantum dot solar cells is much lower for cells fabricated with small quantum dots than with larger quantum dots. The diffusivity is also in the form D=A/X where d is the diffusivity A is a constant and X is the diameter of the quantum dot. This is primarily due to how charges are

transported in a quantum dot film. since the charges must hop from one quantum dot to another, films comprised of small quantum dots will have comparatively more hops than a film comprised of large quantum dots. The number of hops across a film is approximately equal to H=D/X where H is the number of hopes, D is the thickness of the film, and X is the diameter of the quantum dots. The larger the quantum dots, the fewer the hops.

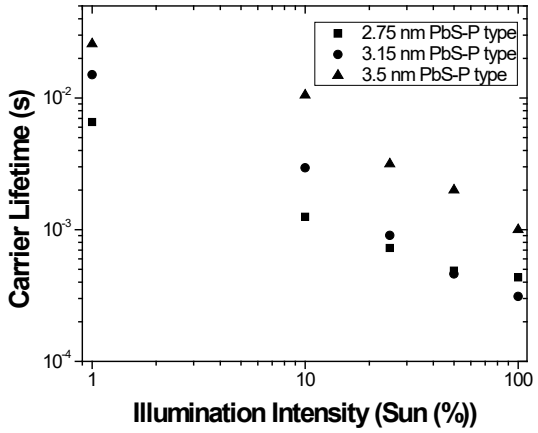


**Figure 29 the minority carrier lifetime is shown for PbS quantum dots of various sizes.**

Shown in figure 29 is the minority carrier(electron) lifetime for P type PbS with varying quantum dot sizes. The minority carrier lifetime is the average time the minority charge carrier is in an excited state before is losing its energy and falls into the ground state. The carrier lifetime is inversely proportional to the defect density of the semiconductor. Defects include impurity atoms as well as grain boundaries. For smaller quantum dots, the electron lifetime significantly shorter than the electron lifetime of larger quantum dots. This is primarily due to an increase in the surface area between quantum dots. The larger surface area creates more surface trap states leading to a higher defect density.

### 4.3.3 Effect of PbS thickness on solar cell performance

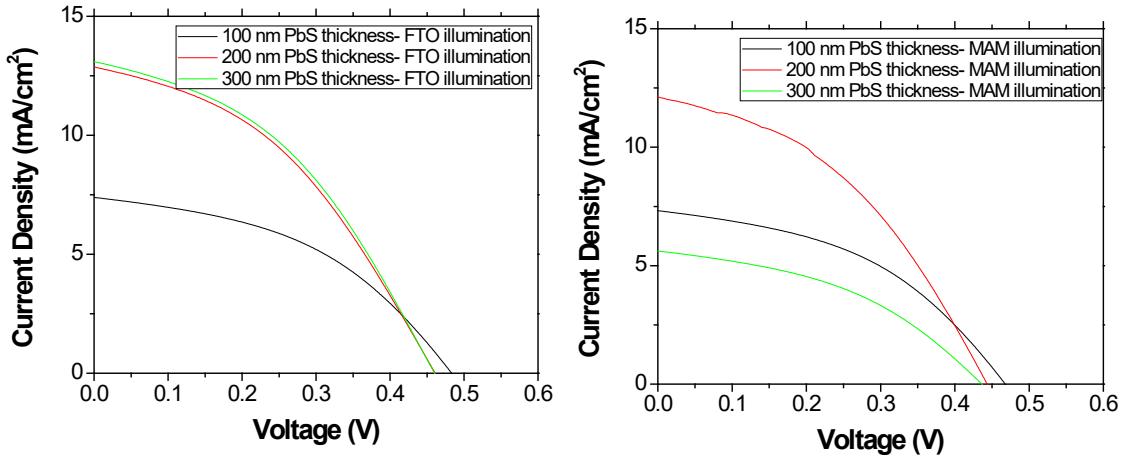


**Figure 30 IV curves of solar cells fabricated with three different thicknesses of PbS active layer through front and back illumination.**

To further show there is a large difference between hole and electron transport in P type PbS quantum dot films, the PbS layer thickness was varied. With a thin PbS quantum dot absorption layer (100 nm), both holes and electrons must travel a very short distance so differences in charge transport behavior will not be noticeable. To make the difference between hole and electron transport more apparent, the thickness of the PbS active layer was increased by a factor of 2 and 3. The increased the lengths charge carriers would have to travel to be extracted. Since the number of extracted charges decreases exponentially with an increase charge transport distance, there will be a large difference in extracted current if the mobilities of holes and electrons differ.

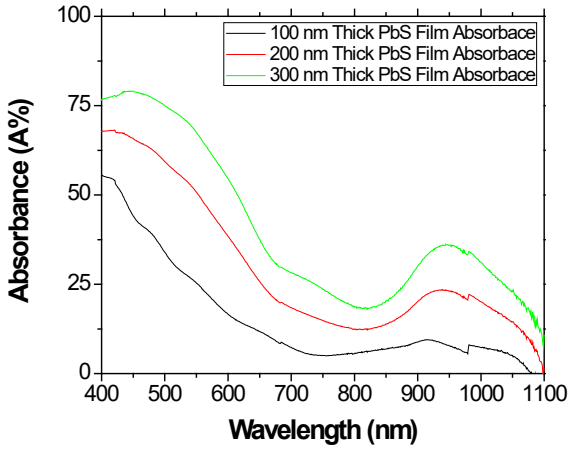


**Figure 31 Absorbance of PbS films with 100, 200, and 300 nm thicknesses**

From figure 30 are the IV curves of PbS quantum dot solar cells with 100, 200, and 300 nm absorbance layers. For the FTO illuminated devices, hole dominated transport, 100 nm of PbS shows the lowest current followed by 200 then 300 nm. The low current for the 100 nm PbS samples is due to the poor light collection. Not enough photons are absorbed by the active layer to produce a high current in the solar cell. PbS solar cells with a 200 nm film thickness is enough to absorb the majority of photons without suffering from a severe increase in recombination. The 300 nm PbS film absorbs more light than both the 200 and 100 nm film however, the extracted current is not much higher. This shows the tradeoff between light absorption and carrier collection in PbS quantum dot solar cells. For devices illuminated through the MAM direction, electron dominated transport, the 100 nm again shows a low extracted current with short circuit current values matching very closely with the FTO illuminated IV curves. The devices fabricated with 100 nm PbS thick absorber films are limited by light absorption for both electron and hole transport dominated testing conditions.

For PbS solar cells fabricated with 200 nm PbS films, the difference in solar cell performance between FTO and MAM illumination is still quite small. This is because the thickness

of the PbS quantum dot layer is less than the diffusion length for both holes and electrons. Both holes and electrons that are generated have a high chance of being transported out of the cell without recombination occurring.

The solar cells fabricated with a 300 nm PbS film offers a better look into the difference between hole and electron transport in these devices. For FTO illumination, hole transport limited devices, the extracted current remains quite high. even though the light absorption of the solar cell increases shown in figure 31, the extracted current does not increase as well. Even though the number of charges generated increased in the solar cell, the number of charges being recombined also increases as they have to travel farther out of the cell.

For electron transport limited devices, MAM illumination, the solar cell performance suffers greatly. The light absorption for the solar cell is the same however, the recombination rate and energy loss in the cell increases compared to the FTO illuminated devices. This is due to the limitations of electron transport in the PbS solar cell. The electron diffusion length in P type PbS quantum dots is approximately 200 nm where the hole diffusion length is 300 nm. Most of the generated electrons will recombine before they travel the 300 nm thick PbS absorption layer resulting in poor current extraction for MAM illumination.

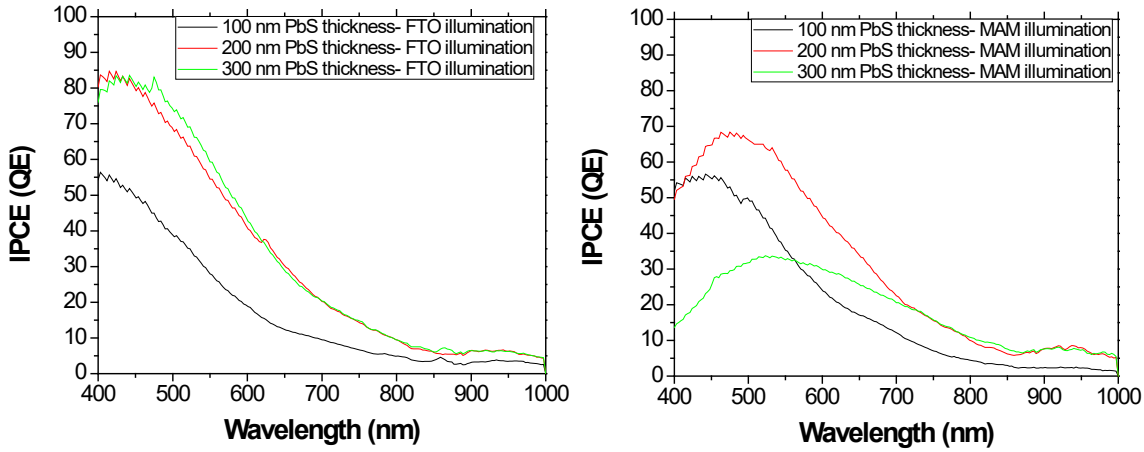


**Figure 32 IPCE measurements of 100, 200, and 300 nm thick PbS quantum dot solar cells illuminated from two directions**

The IPCE measurements for increasingly thick PbS quantum dots show a similar trend to what was found during IV measurements. For MAM illumination, photons with high have a low chance of extraction due to the relatively far distance electrons must travel in the low mobility quantum dot film.

### 4.3.4 Effect of P/N junction on Charge Transport

What was studied next is how the addition of a P-N junction affects the transport properties of charges in P/N type PbS. Since the addition of a P-N junction in the quantum dot film, device performances have been greatly improved. Shown in figure 33 and table 3, are the device

properties of P-N type PbS with different junction locations and the cross section of the cells shown in figure 33d.

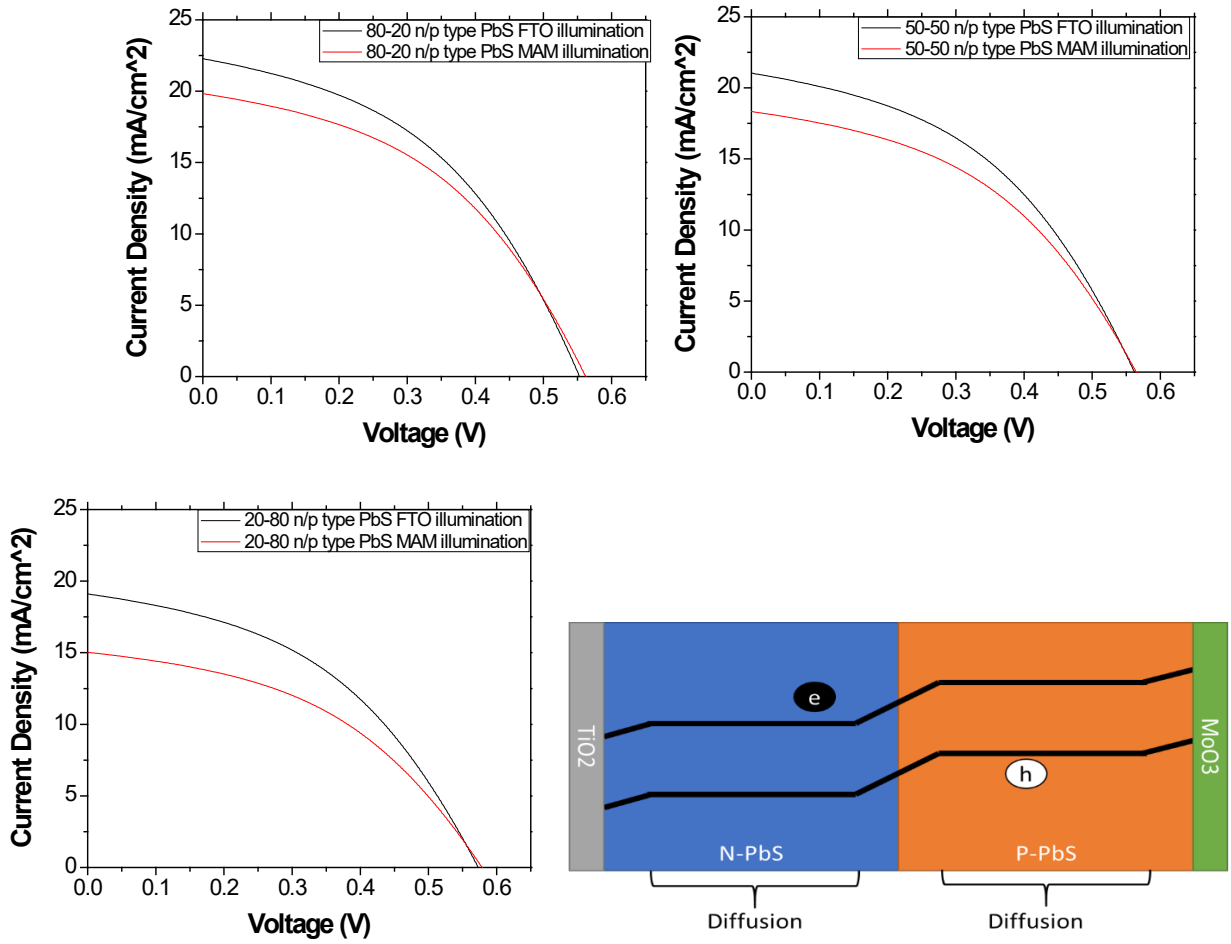


**Figure 33 IV measurements of fabricated PbS solar cells illuminated by two directions. the PbS active layers are comprised of N and P type quantum dots with different ratios of P and N type PbS but the same active layer thickness.**

**Table 3 Qualitative metrics of fabricated P/ N type PbS solar cells in figure 29:**

| PbS Cell | Jsc (mA/ $cm^2$) | Voc (V) | N (%) | FF |
|---|---|---|---|---|
| 20-80 n/p-FTO illumination | 22.27 | 0.553 | 5.37 | 0.436 |
| 20-80 n/p-MAM illumination | 19.82 | 0.563 | 4.88 | 0.437 |
| 50-50 n/p-FTO illumination | 21.03 | 0.562 | 5.18 | 0.437 |
| 50-50 n/p-MAM illumination | 18.33 | 0.566 | 4.53 | 0.440 |
| 80-20 n/p-FTO illumination | 19.10 | 0.574 | 4.82 | 0.448 |
| 80-20 n/p-MAM illumination | 15.06 | 0.578 | 3.33 | 0.440 |

Between pure p and pure n samples previously described, the current extracted from these devices is much higher aided by the addition of a P-N junction. Also, for high P type ratios, the difference between MAM and FTO illumination is much smaller than the pure P type ration. Even though this is 80% P type the difference between front and back illumination is 85% compared to 73% with just P type PbS. This shows that with the addition of even a small N type layer, the formation of a P-N junction improves the charge transport properties of the device significantly as a section of the PbS film is influence by a drift region in the middle of the film shown in figure 33.

To qualitatively explain these differences, the kinetics of holes and electrons were measured through transient current decay measurements under dual light illumination techniques. Shown in figure 33 abc and table 3 are the results of that study. All of the transient decay curves in figure 34 are close together and within an order of magnitude to each other. These results resemble the performance of the extracted iv curs. The current extracted is the combination

between light absorption and charge transport. Since the light absorption is the same for all of the devices as the thickness of the PbS active layer is the same, the difference in device performance is due to charge transport and the kinetic differences between holes and electrons.

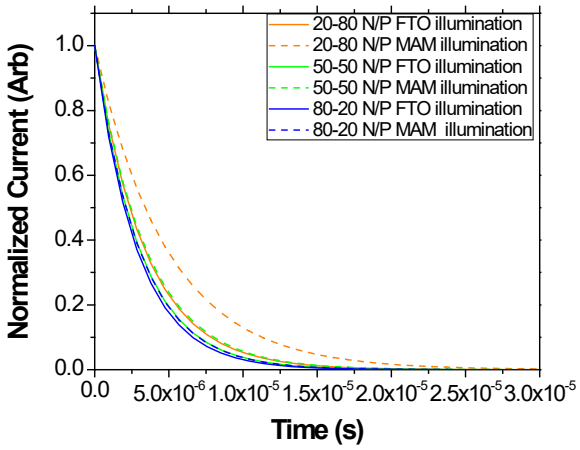


**Figure 34 Current decay constants of P/N type PbS films with different ratios of N and P type PbS**

The measured quantum efficiency shown in figure 35 matches with previously recorded hole and electron kinetic differences.

Blue wavelengths= high light absorption = charge transport difference between holes and electrons is exaggerated clear for high P type PbS ratios large difference between the extracted current between FTO and MAM illumination directions.

Long wavelengths, absorbed deeply into the solar cell active layer, less of a difference between hole and electron transport, the quantum efficiency for all samples tends to become smaller as the wavelength of light increases.

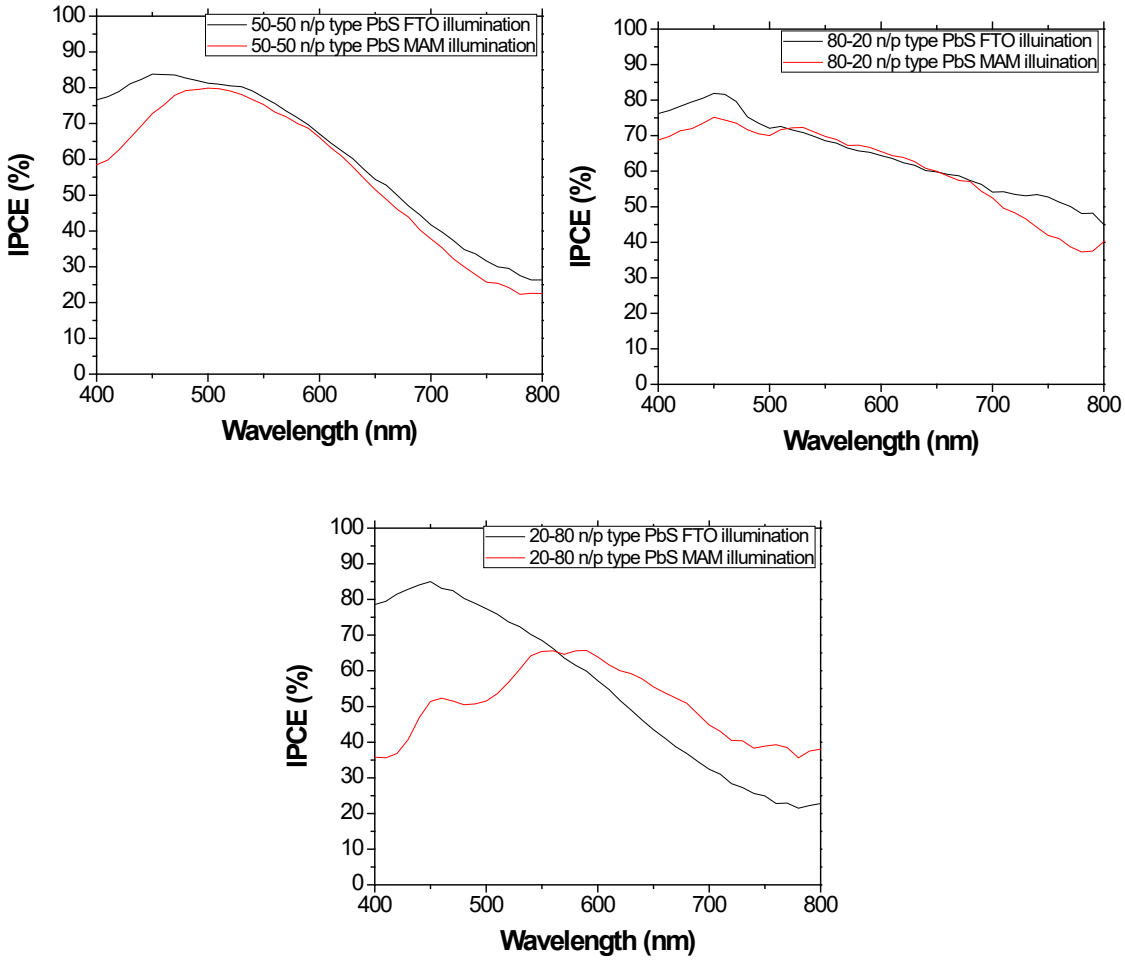


**Figure 35 IPCE measurements of N/P type PbS films with different ratios of p and n type Quantum Dot films.**

The difference in hole and electron transport in solar cell devices can be determined though the unique dual illumination pioneered in the reported data. This is owed to the exponential decay of light intensity and charge generation rate in semiconductor devices and the asymmetrical paths holes and electrons take in a solar cell device. We have found that hole and electron transport in P type PbS devices is preferential to hole transport. This can be elucidated by the lower extracted current from electron limited transport illumination as well as the longer transient times found through current decay measurements. Hole and electron transport kinetics in N type PbS did not appear to be significantly different and that is shown in the small difference in device performance between FTO and MAM illumination directions.

With the addition of a P/N junction in the active layer of the quantum dot solar cell. Measured charge carrier transit times normalize between hole and electron transport. The addition of a drift region in the middle of the active layer, reduces the transport diffusion distance for both charge carriers.

The reason why there is an asymmetrical transport properties between holes and electron in P type PbS and symmetrical transport in N type PbS might be due to the difference in effective mass between holes and electrons in these semiconductors.

# 5.0 Tamm Surface Plasmon influence on PbS quantum dot solar cells

## 5.1 Experimental background

### 5.1.1 Experimental set up

My research will study how metallic thin films affect solar cell performance as opposed to plasmonic nanoparticles. The advantage of using metallic thin films over nanoparticles is the metal film can cover the whole area of the solar cell and increase the amount of semiconductor is affected by the plasmonic resonance from the metals films. One issue with using just a thin metal film as a plasmonic source is light will not be absorbed by the electrons in the metal. We have discovered that Bragg mirrors can be used as substrates for the metal film.[94, 96, 101-104, 143]

### 5.1.2 Plasmonic Solar Cell Design:

To utilize the plasmonic substrates, solar cells must be engineered on top of the substrates to allow for efficient charge transport in the solar cell, so the plasmonic substrate can generate surface Plasmon resonance, and so the PbS solar cell's device performance can be improved by the generation of plasmonic fields. To do this, the following device has been proposed with careful consideration of the above requirements in minds

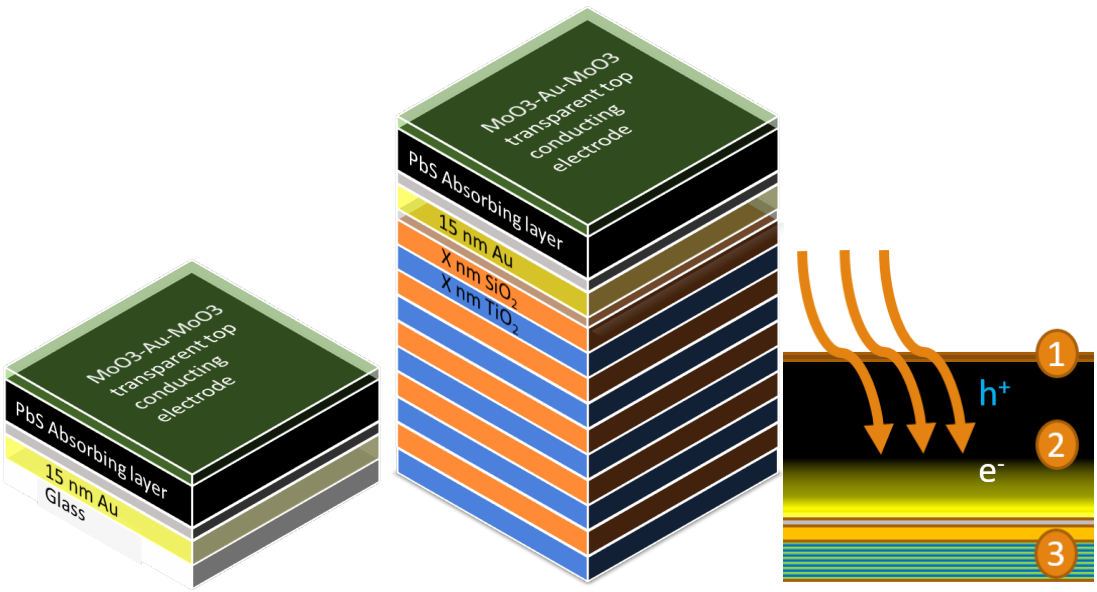


**Figure 36 Cross section of a PbS quantum dot solar cell fabricated on plasmonic thin films**

The device shown in figure 36 was designed with both device performance and actual feasibility of fabrication in mind. The engineering constraints in mind are for preserving the integrity of each film that was previously deposited. There are three sections making up the device, the first labeled 1 in figure 36 is the transparent conductor that allows for light to pass through as well as charges to be conducted out of the device. Section 2 is the PbS active layer that absorbs light and generates charges. Section 3 is the plasmonic thin film that is the source of a local electric field. The plasmonic source and PbS active layer must be in very close contact so the near field effect can influence the light absorption properties of the PbS film.

1. Bragg mirror and surface plasmon source: since the Bragg mirror is the first film that is being deposited, there are few engineering constraints that need to be worked around. Since glass is the substrate the Bragg mirror is going to be deposited on, the only consideration will be to keep the deposition temperature below the softening temperature of the glass. For sodium borosilicate glass, the softening temperature is around 550 °C. To make the

dielectric films of the Bragg mirror, Sputtering was used to deposit $SiO_2$ and $TiO_2$ layers at 500 °C. Sputtering was chosen as a deposition technique due to the large and uniform deposition area and the films can be made relatively quickly and the refractive indexes of the films will be maintained.

2. Electron transport layer: the role of electron transport layers is to provide directionality to generated charges in the absorber layer and to transport excited electrons out of the PbS film. When light is absorbed by semi-conductor films, both holes and electrons are produced. Electron transport layer block holes from leaving the PbS film at the $TiO_2$/ PbS interface. Electrons can freely flow the electron transport layer and holes are forced to travel the opposite direction. Electron transport layers must have few defects to allow for efficient charge transport through the film and so there are no leaks to allow for hole transport though the film. One of the major design constraints for electron transport layers in this structure is the layer must be thin. The plasmonic field from the underlying metal fields decay exponentially with distance from the film increases. If the electron transport layer is too thick, the plasmonic field will decay quickly and there will be no effect on above PbS absorption layer. Due to constraints with temperature as well as strict film morphology requirements, traditionally solution processing followed by a high temperature annealing step will not be possible. To form a dense and thin electron transport layer, ozone assisted atomic layer deposition will be used. Atomic layer deposition is a cyclic deposition method that reacts precursors on the surface of substrates to slow build up a film. Due to the intrinsic nature of the deposition method, film defects are lower in an ALD grown film than a one-step deposition process such as solution based methods. Ozone assisted ALD was chosen as an oxidant because it makes a more crystalline and contaminant free film

than using water as an oxidant. The thickness of the grown film will be 15 nm and will be grown at 250 °C.

3. PbS film: As summarized previously, as the film thickness is increased, more light is absorbed by the PbS film increasing the amount of charges generated in the film. as the film thickness increases, the farther the charges generated in the PbS film must travel. For this plasmonic solar cell design, another consideration must be taken into account. Since the light travels through the PbS film before it makes contact with the metal plasmonic film, if all of the light is absorbed by the PbS film, there will not be any surface Plasmon's generated by the underlying metal film as light cannon reach the metal film to excite it.

Another consideration in terms of PbS film fabrication is the size of the PbS quantum dots. As the size of the quantum dots is changed, the absorption spectra will also change. Large quantum dots will decrease the bandgap back to bulk values. The electron and hole levels will also change accordingly. To maintain a positive energy gradient for electron and charge transfer out of the solar cell from the PbS to the electrodes, the minimum band gap can be calculated to be 1.1 eV. By increasing the bandgap by fabricating small PbS quantum dots, the open circuit voltage will increase slightly however current the extracted current will be lower due to limiting the wavelengths of light can be absorbed. Also, due to the discrete nature of PbS quantum dot allowed energy states, the absorption spectrum is not the same as traditional solar cells. PbS absorption has a peak near the band gap and then the absorption decreases to a valley at lower wavelengths due to a reduction in the allowable energy level transitions from the valance band to the conduction band.

4. Transparent top contact: the top contact needs to be conductive, transparent, and able to effectively transport holes out of the PbS layer. Also, since the PbS film is sensitive to temperature and atmosphere, needs to be able to be deposited around room temperature and in an invert or vacuum environment. Traditionally, FTO or ITO would be used as transparent conducting layers however depositing these thin films requires high processing temperatures that would destroy the underlying PbS layer. Dielectric-metal-dielectric films are popular conductive/transparent films that can be made at room temperature. In the DMD structure, the thin metal film is the primary conductive layer. If just a thin metal layer was used, the transmittance would be low due to the high reflectance of the metal film. by sandwiching the metal between two dielectrics, free oscillating electrons causing the reflectance are kept from oscillating making the film transparent. The dielectric also needs to be electrically compatible with the PbS layer and able to extract holes out of the solar cell. $MoO_3$ has been heavily studied as a hole transport layer for PbS quantum dot solar cells and can be deposited through ebeam evaporation at room temperature. For a metal film in the DMD layer, gold will be used as it's work function is compatible for hole extraction.

## 5.2 Experimental procedures

### 5.2.1 Solar Cell Fabrication

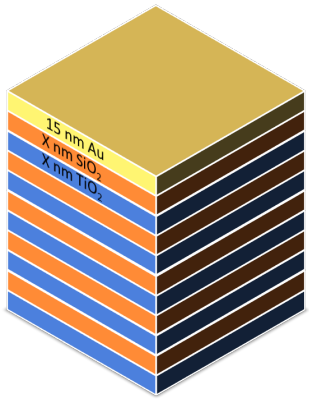


**Figure 37 Completed Tamm surface plasmon thin film comprised of a $TiO_2$ and $SiO_2$ Bragg mirror and a thin gold film.**

A Bragg mirror is comprised of multiple alternating layers of high and low refractive index materials. For this application, $TiO_2$ and $SiO_2$ were used as the high (n=2.3) and low (n=1.5) refractive index materials. To deposit these films, sputtering was done at 500 °C on a glass slide substrate. $TiO_2$ films were sputtered by DC sputtering Ti metal while introducing oxygen to the argon ion flow. $SiO_2$ films were sputtered by RC sputtering a $SiO_2$ target. Target thicknesses were controlled by adjusting deposition time. The Thicknesses used for dielectric layers in plasmonic films are 80, 100, and 120 nm these correspond to Bragg wavelengths of 600, 750, and 900 nm.

The 15 nm gold thin film was deposited through ebeam evaporation at a rate of 0.5A/s and vacuum of 1E-6 Torr. Prior to gold deposition, a 3 nm Cr layer was deposited to promote adhesion of the gold film to the oxide surface of the Bragg mirror. Without the Chromium adhesion layer,

the gold film will easily detach from the oxide layer of the Bragg mirror. This is because the interfacial energy between oxides and gold is high due to the preference of gold to not form an oxide.

A 2 nm Ti film was deposited on the gold film as a seed layer for further $TiO_2$ growth through ALD.

A 10 nm $TiO_2$ electron transport layer was deposited through atomic layer deposition using TDMA-Ti and ozone at 250 °C and 10 mTorr. Purge times were 10 seconds for both precursors, and $TiO_2$ growth rate is 0.45 A/cycle.

### 5.2.2 PbS quantum dot fabrication

Materials: Octadecene(ODE) technical grade, PbO 99.99%, Oleic acid (OA) 97%, TMS all reagents were purchases through fisher scientific. Acetonitrile, EDT

PbS quantum dots with an absorption peak at 900 nm were fabricated by an adjusted recipe pioneered by Hines and Scholes.[69] Prior to synthesis ODE was degassed under vacuum at 85 °C for 12 hours. 450 mg of PbO, 18 ml of ODE, and 1.5 ml of OA were mixed in a three-neck flask under vacuum at 70 °C for 3 hours. Under air free Scheck line conditions, the atmosphere of the flask was switched to nitrogen and the temperature was raised to 95 °C for an additional hour or until the mixture became clear. A syringe of 10 ml of ODE and 207 uL of TMS was prepared as the temperature of the flask was raised to 115 °C. The flask was removed from an oil bath while the temperature of the solution was monitored with an in-situ thermal couple. To initiate PbS nucleation, the syringe of ODE and TMS was swiftly injected into the PbO-Oleate mixture. What follows is the sudden drop in temperature and the nucleation of black PbS quantum dots. The

solution cooled naturally to room temperature under nitrogen flow prior to purification. The quantum dots were separated from the reaction byproducts through centrifugation with acetone. This solution was then dispersed in hexane and stored in a low humidity desiccator. Prior to PbS film deposition, the PbS solution was further purified by centrifuging the quantum dots in a 1:1 mixture of acetone and methanol and drying over nitrogen. This process was repeated three times before the PbS was dispersed in hexane with a concentration of 25mg/ml.

### 5.2.3 Solar Cell fabrication

To form PbS quantum dot films, spin coating was performed in a low humidity (H<20%), nitrogen filled glove box. For a spin coating cycle, the fabricated plasmonic substrates were spun at 2500 rpm. 40 ul of PbS in hexane was spin cast on the surface of the substrate, 80 ul of 2 V/V% of EDT in acetonitrile was spin cast to exchange the native oleate ligands with short thiols, finally, 80 ul of Acetonitrile was cast on the spinning substrate to clean the film. Each Spin coating cycle deposited 20 nm of PbS and was repeated to build up a film.

The top contact was deposited through ebeam evaporation under vacuum of 1E-6 Torr at a rate of 5 A/s for $MoO_3$ and 0.5 A/s for Au. 10 nm of $MoO_3$, 10 nm of Au, and 10 nm of $MoO_3$ were deposited in series to form a dielectric-metal-dielectric conductive/transparent contact.

The solar cell active area was 0.0375 $cm^2$ (1.5x2.5 mm) which was controlled by the overlap of the bottom gold film and the top M-Au-M layer.

Absorption and scattering measurements were performed with a Perkin Elmer Lambda 950 spectrophotometer with a 150-mm-diameter integration sphere. The use of an integrating sphere allows for the capture of light from diffuse and specular reflectance. Absorption was calculated by measuring reflectance and transmittance and subtracting from unity. JV-curves were recorded by

an electrochemical workstation while devices were illuminated under AM1.5G (100 Mw/ $cm^2$, Oriel Newport). IPCE measurements were done under a Newport system using a Si solar cell as a reference photodetector. The system used a mercury lamp as a white light source and a monochromator to isolate the desired wavelength.

## 5.3 Results

### 5.3.1 Effect of changing Tamm Plasmonic peak position

This study will determine the effect of changing the Tamm surface plasmon wavelength and what affect that has on the opto-electronic properties of the PbS solar cell. By changing the surface plasmon wavelength, the wavelengths of light that will be influenced will also change.

#### 5.3.1.1 Reflectance of Bragg mirrors

The reflectance of fabricated Bragg mirrors are shown in figure 39. As the thickness of the dielectric layer's increase, the maximum reflectance peak also increases according to equation 5.1. When the layer thicknesses are 80 nm, the Bragg wavelength is 600 nm. When X=100 nm, the Bragg wavelength is 750 nm. When X=120 nm, the Bragg wavelength = 900 nm. Using three different wavelengths will allow us to determine how different regions of light impact PbS quantum dot solar cell performance. The PbS quantum dot used in this experiment is 1.37 eV corresponding to an absorbance peak of 900 nm. By using this quantum dot size, the Bragg wavelength of previously described films correspond to strong absorbance regions at low

wavelengths at 600 nm, poor light absorbance regions of the PbS at 750 nm and the quantum dot absorbance peak at 900 nm for the Bragg mirror with the thickest dielectric layers.

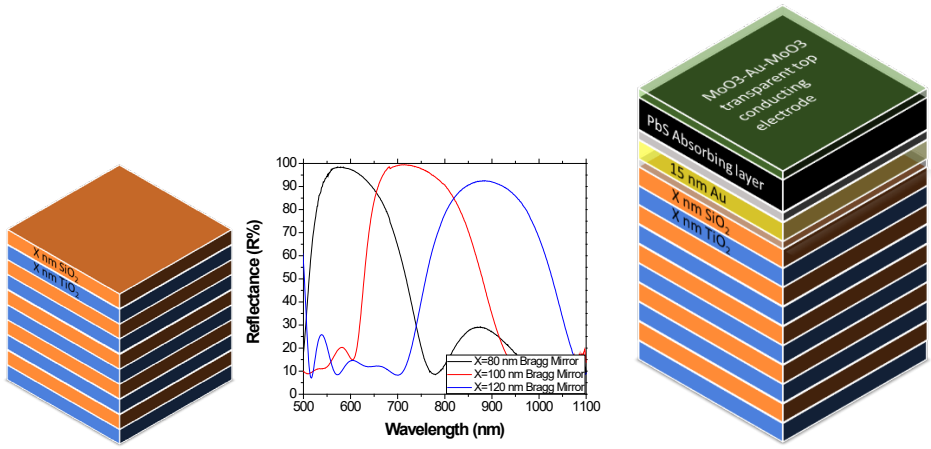


**Figure 38 Bragg mirrors fabricated with 80, 100, and 120 nm $SiO_2$/ $TiO_2$ dielectric layers. The cross section of the Tamm surface plasmon assisted PbS quantum dot solar cell.**

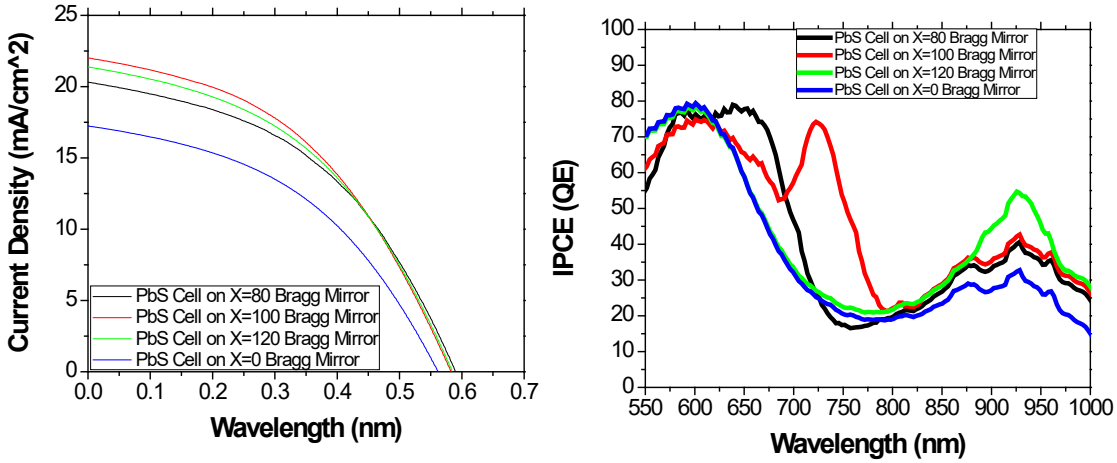


**Figure 39 Opto-electronic testing of PbS solar cells with underlying plasmonic thing films b) IPCE performance of plasmonic and non plasmonic PbS quantum dot solar cells**

From figure 40 and table 5, with the addition of a Bragg mirror under a thin gold film, the exacted current density has increased by 18%, 27%, and 22% for X=80, 100, and 120 nm dielectric layer thicknesses. The Fill factors do not differ between X=0 and the plasmonic samples. There is a minor increase in Voc from 0.567 to 0.585 V between cells without and with an underlying Bragg mirror. This results in a change of solar cell efficiency from 4.24% for X=0 to 5.37, 5.65, and 5.52% for X=80, 100, and 120 nm. The increase in efficiency is mostly due to the increase in extracted current. With the addition of an underlying Tamm plasmonic thin film, there appears to be a significant increase in charge generation rate in the PbS quantum dot devices. To determine why there is an increase in charge generation rate, the quantum efficiency was found through IPCE to determine what wavelengths the QE increased for.

The IPCE for all fabricated cells is shown in figure 41b. All cells have a characteristic peak at 900 nm which corresponds to the PbS quantum dot absorption peak at 900 nm. For cells not fabricated on a multilayer, there are no more peaks only a valley at 700-800 nm wavelengths corresponding to the decrease in light absorbance of the quantum dot films (figure 37). For PbS cells fabricated on multilayer substrates, X=80, 100, and 120 nm, there is an increase in the IPCE at 600, 750, and 900 nm wavelengths, respectively. The peak wavelengths in IPCE correspond to the Bragg wavelength of the underlying Bragg mirrors displayed in figure 39.

For PbS cells fabricated on X=80 nm multilayers, the increase in IPCE at 600 nm from X=0 nm multilayers are from 50 to 80%. For X=100 nm the increase in IPCE at 750 nm from X=0 nm multilayers are from 30 to 75%. For X=120 nm the increase in IPCE at 900 nm from X=0 nm multilayers are from 30 to 60%.

The presence of IPCE peaks show that the Tamm surface plasma effect is causing the solar cell devices to increase the quantum efficiency around tunable wavelengths. All PbS quantum dot

films with Tamm surface plasmon have a peak in their ipce that corresponds to the Bragg wavelength of the underlying Bragg mirror and therefore the existence of Tamm surface plasmon. Since quantum efficiency is a product of light absorption and charge transport, the increase in ipce peaks can be due to either of them. To confirm that the quantum efficiency increased due to local light absorption increases, the absorption spectrum of all devices were found.

**Table 4 Layout of Opto-electronic parameters from IV testing under one sun illumination**

| PbS Cell on X= Bragg Mirror | Jsc (mA/ cm$^2$) | Voc (V) | N (%) | FF |
|---|---|---|---|---|
| X=0 | 17.24 | 0.567 | 4.24 | 0.434 |
| X=80 | 20.32 | 0.589 | 5.37 | 0.449 |
| X=100 | 22.02 | 0.582 | 5.65 | 0.441 |
| X=120 | 21.38 | 0.584 | 5.52 | 0.442 |

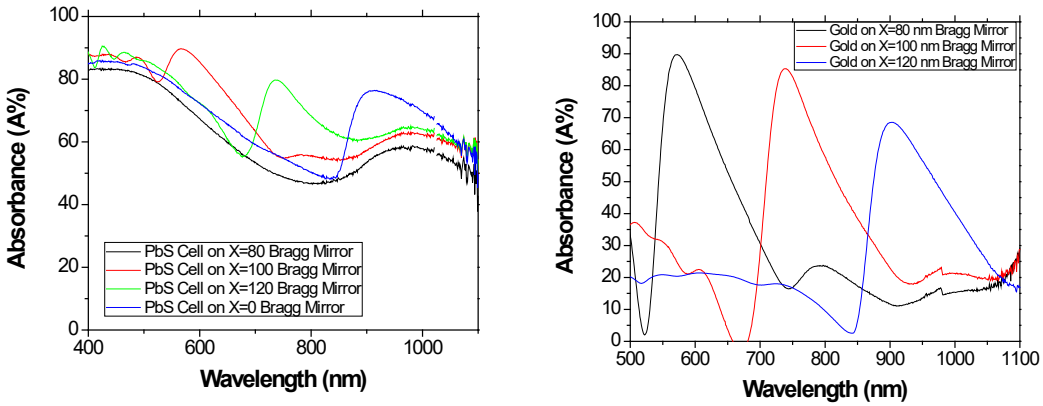


**Figure 40 Absorption of PbS quantum dot solar cells fabricated on Multilayers with 0, 60, 80, and 100 nm dielectric layer thicknesses.**

The absorbance of solar cells with and without plasmonic films are shown in figure 4. All devices show an absorption peak corresponding to the PbS quantum dot absorption peak at 900 nm. The PbS cells fabricated on plasmonic substrates also show another characteristic absorption peak. The peaks are centered at 600, 750, and 900 nm for X= 80, 100, and 120 nm. The increase in light absorption at 600 nm for X=80 nm multilayer is from 60 to 90% absorbance, 750 nm for X=100 nm multilayer is from 50 to 80% absorbance, and at 900 nm wavelength for X=120 nm multilayers from 60 to 80%. The increase in light absorption is catalyzed by the underlying Tamm surface plasmon increasing the local absorption coefficient of the above quantum dot film. The increase in light absorption of the quantum dot film allows for more photons to be captured and therefore more electron hole pairs made. The electrons/holes are extracted from the film and increase the current of the devices. For quantum dot devices, Tamm assisted solar cell devices with an underylying bragg mirror with dielectric layer thicknesses of 100 nm shows the most improvement in terms of extracted current. This is because the wavelength that the Tamm surface plasmon affects is in a wavelength region of 1.37 eV bandgap PbS that has a poor absorption coefficient. It improves the absorption of the solar cell device in regions of poor light absorption leading to a large increase in charge generation. Both the x=80 and 100 nm Tamm surface plasmons have Bragg frequencies that overlap with an already high light absorption region in the PbS film. Therefore, there is not a large possible increase in solar cell performance.

To determine the influence of the plasmonic substrate on the optical absorption of the PbS solar cells, the absorbance of just the plasmonic substrates were found. The absorbance of the plasmonic thin films are shown in figure 4. There are absorption peaks at 600, 750, and 900 nm

for X=80, 100, and 120 nm respectively. It is only when the thin gold and multilayer films are combined is there any significant absorption response.

### 5.3.2 Effect of PbS quantum dot size on Tamm plasmonic assisted quantum dot solar cells

Both the quantum dot and plasmonic absorption spectra can be tuned by changing their geometric properties. This section studied what affect changing the quantum dot absorption peak had on the device performance of a tamm surface plasmon assisted solar cell had when keeping the Tamm wavelength constant. The tamm surface plasmon under study here is centered at 900 nm. This absorption peak occurs when the dielectric layer thickness of the Bragg mirror is 120 nm. The PbS absorption peaks being studies are centered at 800, 900, and 1000 nm corresponding to a bandgap of 1.55, 1.37, and 1.24 eV, respectively. The bandgaps of the particles correspond to a Tamm photon energy of higher than the bandgap, at the band gap, and lower than the bandgap.

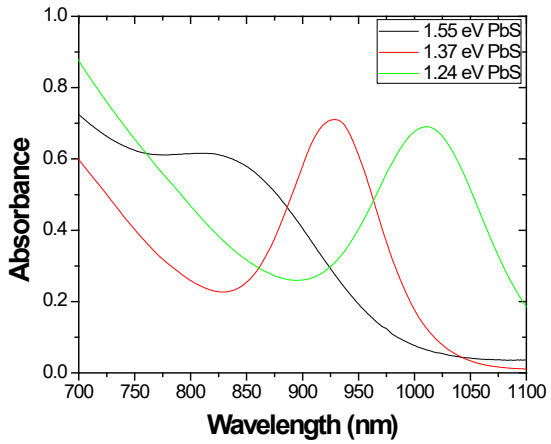


**Figure 41 quantum dot absorption peaks of three different sized PbS quantum dots**

Figure 42 shows the absorption spectra for the three fabricated quantum dots for the whole visible and near infrared range along with a blow up of the normalized absorption peaks of the quantum dot solids.

Tamm surface plasmon assisted solar cells were fabricated using the same method described in the previous sections.

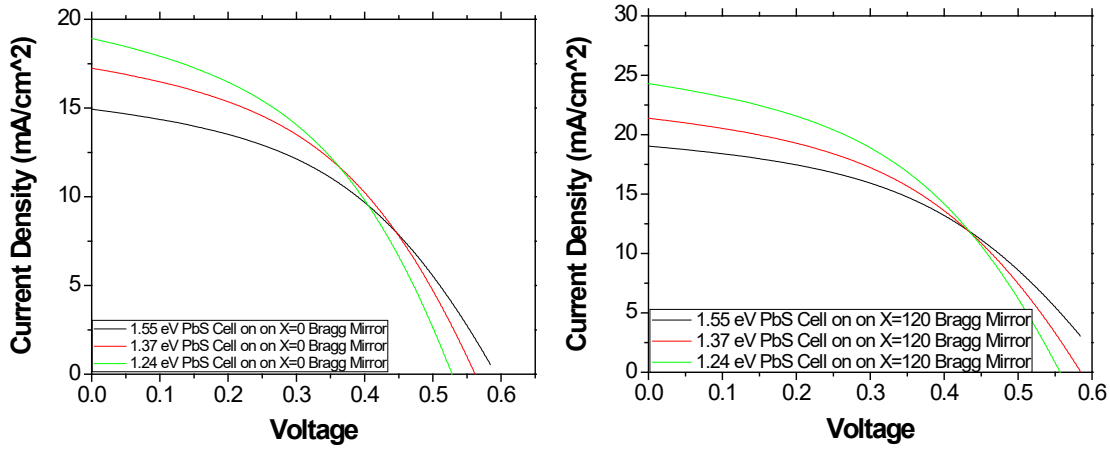


**Figure 42 JV measurements of Tamm plasmon solar cells fabricated with PbS active layers comprised of 1.55, 1.37, and 1.24 eV quantum dots.**

As the quantum dot bandgap increases, there is an increase in open circuit voltage of the solar cell and a decrease in short circuit current density and a slight decrease in fill factor. The metrics for each cell are shown in table 6. The highest performing solar cell device is the 1.37 eV quantum dot film with an efficiency of 4.24% while the 1.24 eV quantum dot has an efficiency of 4.22 %.

**Table 5 Metrics of PbS quantum dot solar cells with 1.55, 1.37, and 1.24 eV bandgaps with and without an underlying Tamm plasmon thin film.**

| PbS Cell X=0 Bragg mirror | Jsc ($mA/cm^2$) | Voc (V) | N (%) | FF |
|---|---|---|---|---|
| 1.55 eV PbS | 14.95 | 0.587 | 3.71 | 0.423 |
| 1.37 eV PbS | 17.24 | 0.567 | 4.24 | 0.434 |
| 1.24 eV PbS | 18.62 | 0.523 | 4.22 | 0.441 |

| PbS Cell X=120 Bragg mirror | Jsc ($mA/cm^2$) | Voc (V) | N (%) | FF |
|---|---|---|---|---|
| 1.55 eV PbS | 16.80 | 0.603 | 4.26 | 0.434 |
| 1.37 eV PbS | 21.38 | 0.582 | 5.52 | 0.442 |
| 1.24 eV PbS | 23.28 | 0.556 | 5.67 | 0.438 |

With the addition of an underlying Bragg mirror with dielectric layer thicknesses of 120 nm, all cells show an increase in extracted current as shown in table 6. The largest increase in solar cell efficiency is for the 1.24 eV quantum dot. Its current density rose from 18.62 to 23.28 mA/ $cm^2$ and device efficiency rose from 4.22 to 5.67 %. The 1.55 eV quantum dot device only showed a small increase in device performance with a current density improvement from 14.95 to 16.80 mA/ $cm^2$. To determine why there is a large device improvement for PbS cell fabricated from 1.24 eV quantum dots but only a marginal increase in device performance for PbS cells fabricated from 1.55 eV quantum dots, IPCE measurements were done to determine what wavelengths the quantum efficiency has been improved for.

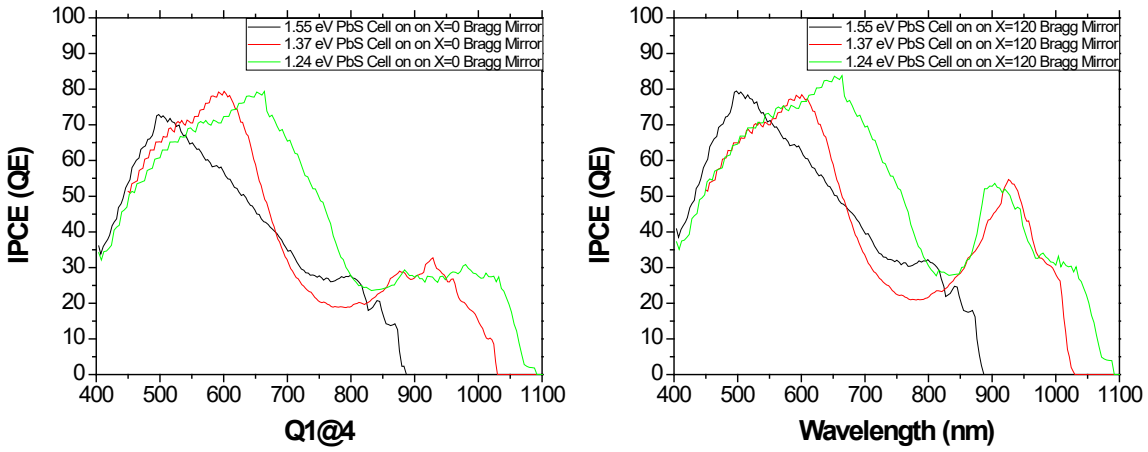


**Figure 43 incident photon conversion efficiency for plasmonic and non plasmonic PbS solar cells with different quantum dot sizes.**

The IPCE of the quantum dot films without Tamm surface plasmon assistance corresponds to the absorbance of the quantum dot film with cutoffs in quantum efficiency at the bandgaps of

the fabricated solar cell devices. Importantly, the cutoff of quantum efficiency for the 1.55 eV quantum dot occurs below 900 nm, the Bragg frequency of the plasmonic film. With the addition of the 120 nm layer thick Bragg mirror, the quantum efficiency for all samples is slightly improved across all wavelength ranges as the reflectance of the Bragg mirror caused light to pass through the PbS film twice increasing its absorption length. The 1.37 eV and 1.24 eV quantum dot devices have IPCE peaks at 900 nm. There is no increase in quantum efficiency at 900 nm for the 1.55 eV bandgap devices. Even though all devices have Tamm surface plasmons, there does not appear to be an increase in IPCE for the 1.55 eV bandgap PbS with the Plasmonic film. To determine the cause of the increase in IPCE for the 1.37 and 1.24 eV bandgap devices but not the 1.55 eV device, the light absorption properties of the devices was found.

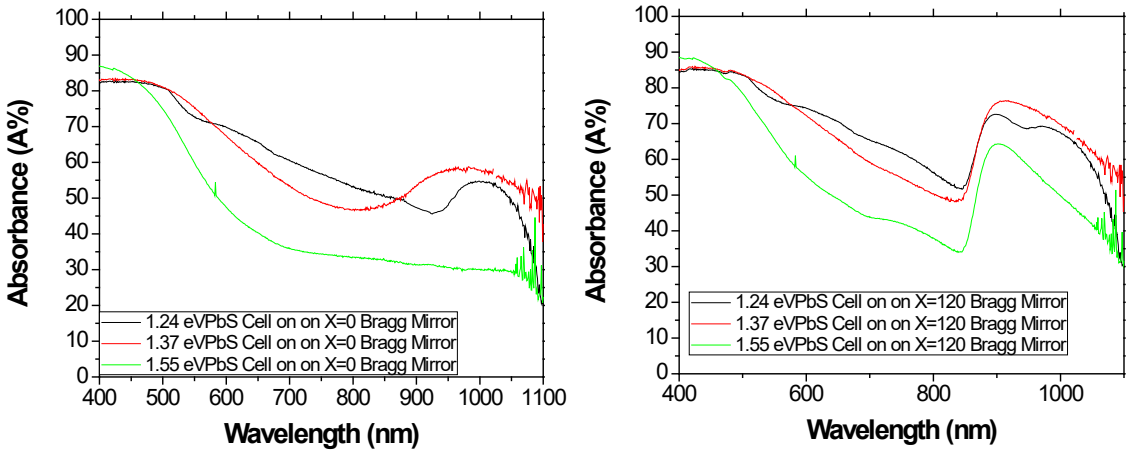


**Figure 44 light absorption of PbS solar cells with different sized quantum dots with and without Tamm plasmon films.**

The light absorption of PbS solar cell with different quantum dot band gaps are displayed in figure 45 a. the light absorption of the films follows the general absorbance of the quantum dots

themselves with visible peaks at 800, 900, and 1000 nm corresponding the absorption peaks of the individual quantum dots themselves.

With the addition of the Bragg mirror, a general increase in light absorption occurs for all wavelength supporting the argument that the Bragg mirror increases the optical length of the Quantum dot film. At the Bragg wavelength of 900 nm, a Tamm surface plasmon is formed and all samples show a spike in light absorption around 900 nm wavelengths.

By tuning the quantum dot size and therefore bandgap, the effect of how the Tamm plasmon thin film increases the light absorption of the above quantum dot film. There are studies that claim plasmons can generate so called hot electrons that can tunnel into the semiconductor and added to the extracted current of the fabricated device. Other studies claim that the presence of the plasmonic field increases the light absorption of the semiconductor itself and the increase in light absorption of the semiconductor itself is the reason for an increase in extracted current. This experiment examined how having a Tamm surface plasmon with a Bragg wavelength with a photon lower than the bandgap of the solar cell active layer affects the quantum efficiency of the deice. We have found that there is no significant increase in quantum efficiency for photons at the Tamm plasmon wavelength with a solar cell with a bandgap higher than the Tamm plasmon of the underlying film. there is however an increase in light absorption of the whole solar cell device. This shows that the Tamm surface plasmon is absorbing light and that light energy is lost to heat as the device does not convert it to usable electricity.

### 5.3.3 Thickness of PbS film

Experiments described in 5.3-3 and 5.3-4 are used to differentiate between the near field and far field effects of the plasmonic thin films. The far field effect simply reflects light off of the

back of the contact and increases the optical pathway of the active layer. The near field effect is caused by the presence of local electric fields centered at the metal film that decay exponentially into the PbS active layer. The electric field improves the local absorption coefficient around the Bragg wavelength of the Tamm plasmonic film and allowing for charge generation in a device.

To find the effects of the near field effect, 3 different thicknesses of PbS films were used. A thin device that shows strong light absorption and IPCE peaks at the Bragg wavelengths shows that the Tamm surface plasmon affects solar cell active layers very close to the gold thin film. A thick PbS film will have high absorption across all wavelengths but the impact of the Tamm surface plasmon will be diminished compared to a thin PbS film as the near field affects the semiconductor film locally.

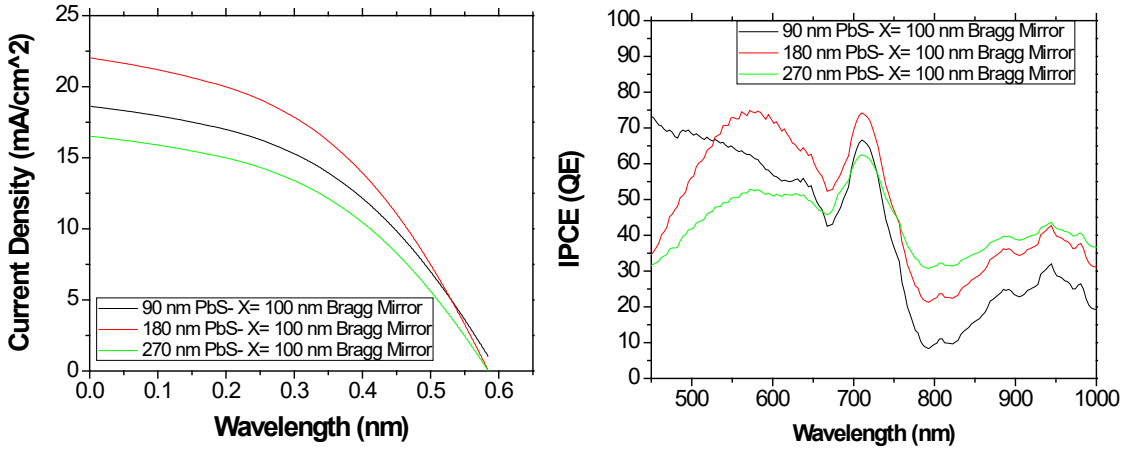


**Figure 45 Opto-electron measurements of PbS quantum dot solar cells with increasing PbS film thickness**

In order to determine how light absorption is enhanced in the quantum dot solar cell by the simple far field effect caused by back contact reflection and through the influence of the near field effect from Tamm surface plasmons, different PbS film thicknesses were used as active layers in

solar cells. Using X=100 nm multilayers, the quantum dot film thickness was 90, 180, and 270 nm. The increase in PbS film thickness will increase the overall light absorbance across all wavelengths shown in figure 47. Looking at the IV curves of the fabricated devices, the highest performance cell has a film thickness of 180 nm and the poorest performing device has a film thickness of 270 nm. Looking at the IPCE, all cells show a peak in the ipce at 750 nm which corresponds to the plasmonic Bragg wavelength of the underlying films. The IPCE values are most different at high and low wavelengths however, at blue wavelengths, the IPCE is highest for thin PbS films and lowest for the 90 nm PbS film. At high wavelengths, >800 nm, thick PbS films have a higher IPCE than thin wavelengths PbS as light absorption is higher in this region.

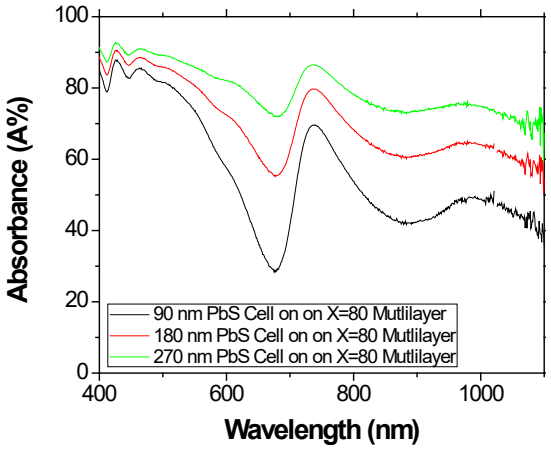


**Figure 46 Light absorbance of PbS cells on plasmonic thin films.**

Even with a thin PbS active layer of 90 nm, the quantum dot solar cells show high light absorption at the Bragg wavelength of 750 nm. The quantum dot active layer is absorbing the light and not the metal film itself as the quantum efficiency peak matches the absorption peaks of the device. This shows that the Tamm plasmon near field effect can have significant effects on device performance even though the active layer is thin. On the opposite side, the light absorption is

higher for all wavelengths as the light has a farther optical pathway to travel though the semiconductor. This does not translate to higher quantum efficiency however, this is because charges generated by the PbS film recombine before they are extracted due to the additional charge transport length. This leads to a lower overall current and device efficiency due to recombination. The thicker PbS film also reduces the effectiveness of the plasmonic thin film as light is already absorbed by the PbS film before it reaches the near field effect area. There exists and optimal film thickness that has high charge transport properties and light absorption for all wavelengths in the device.

### 5.3.4 Far Field Reflectance vs Near Field Effect

The purpose of this experiment is to determine the effect of far field reflection on the device performance of the quantum dot devices. Using a thick gold film as a reflective back contact, reflectance will be maximized across the wavelength spectrum and an increase in light absorption will be due to reflection and not Tamm surface plasmon effects. Using a thin gold film will have minimal reflectance across the solar spectrum.

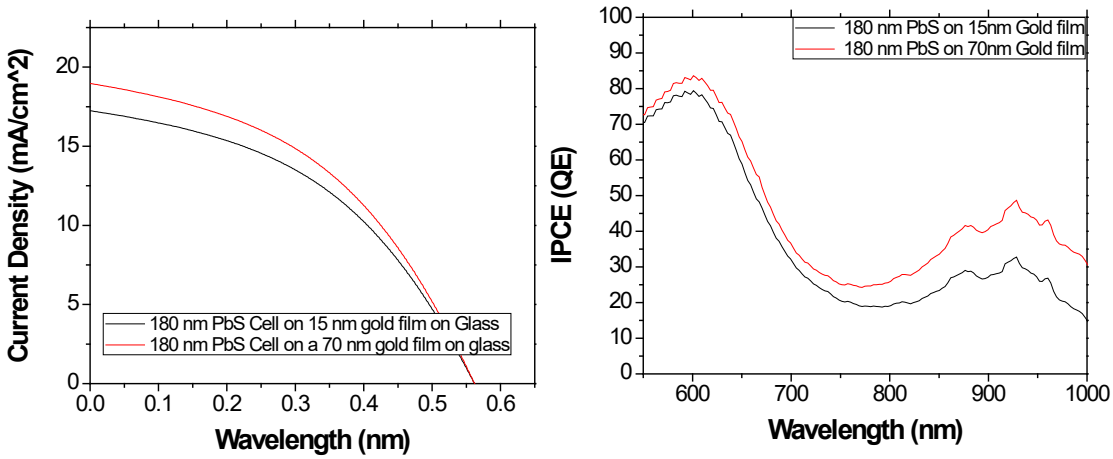


**Figure 47 Opto-electronic measurements of PbS cells fabricated on thin and thick gold layers**

The purpose of this experiment is to determine how much of an influence a back reflective contact has on the device performance of PbS quantum dot solar cells. A 70 and 15 nm Au film was deposited as a bottom contact for PbS quantum dot solar cells. The reflectance of both contacts is shown in figure 48. The reflectance of the 15 nm PbS film is only 30 % and the reflectance for the 70 nm film is approximately 100% for wavelengths higher than 500 nm. The absorbance of PbS cells fabricated with these back contacts is shown in figure 8a. the absorbance of the PbS cells made on the thick gold film is higher than the thin gold film across all wavelengths with the highest difference occurring at wavelengths greater than 700 nm. The increase in light absorbance increases the overall cell efficiency for the 70 nm thick gold sample as the current increases from 17 to 19 mA/ $cm^2$. The IPCE confirms this behavior as the quantum efficiency for 70 nm Au back contact is higher past 700 nm.

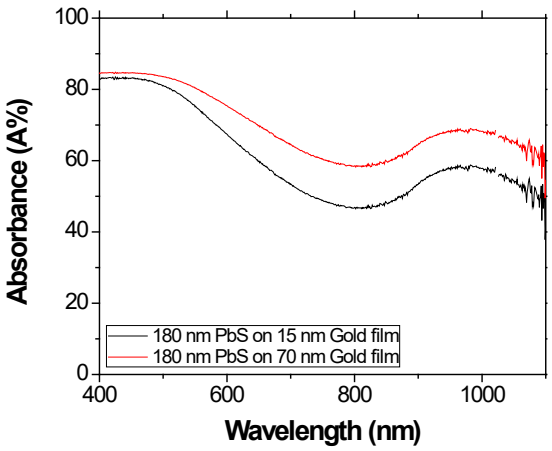


**Figure 48 Absorbance of PbS quantum dot solar cells fabricated on thin and thick gold layers**

The secondary influence plasmonic thin films have is the increase in light absorption due to far field reflectance effects. The use of the thick gold layer maximized the far field effects as its reflectance is effectively 100%. Even though he reflectance of the back contact is high the improvement in absorption is not as significant as with the Tamm surface plasmons. The high reflectance of the thick gold layer effectively doubles the optical light path in the PbS film. This shows that both near field and far field effects influence the opto-electronic properties of PbS solar cells.

### 5.3.5 Conclusion

The plasmonic waves only significantly affect the quantum dot film near the plasmonic contact. This can be seen using a thin PbS active layer. Even though the active absorbing layer is thin, when accompanied by a plasmonic thin film, the ipce and absorbance of the solar cell remains high at the Bragg wavelength. This shows that even with a thin absorbing layer, the Tamm surface

plasmons allow for an optically thick virtual film while the actual PbS quantum dot film remains thin. This improves the light absorption properties of PbS solar cells while still limiting recombination and reduction in charge transport.

The effectiveness of the utilization of the plasmonic film is dependent on which wavelength it is tuned to. If wavelength is tuned to low wavelength where absorption in the PbS film is already high, the improvements to the absorption and IPCE are marginal. By placing the Bragg wavelength in the middle of the absorption valley, the greatest quantum efficiency improvement can be found. This principle remains true as the thickness of the PbS film increases. Even in the region of poor light absorbance, the increase in PbS thickness increased the overall absorption of the solar cell however, the charge transport properties of the solar cell decreased as the average charge transport distance also increased. This leads to a decrease in overall solar cell performance.

We have also showed in two different experiments that the Tamm surface plasmon effect can be tuned to improve the light absorption in semiconductor films by adjusting the Tamm surface plasmon wavelength as well as the absorption spectra of the quantum dot film by changing the quantum dot size.

Increase in light absorbance does not necessarily increase the carrier collection efficiency. Above bandgap must be compatible with absorbing the photon energy of the incoming photon.

The underlying Bragg mirror can be tuned to generate surface plasmons at any wavelength above the plasma frequency of gold. What was not studied in this report is how other plasmonic active metals such as aluminum or silver may influence the optoelectronic response in PbS solar cells. This study also focused on direct bandgap semiconductors. Traditionally, indirect band gap silicon is used as the function material for commercial solar light harvesting. The limitation in light absorption in silicon is owed to the change in electron momentum required for photon absorption.

It is undetermined if the presence of Tamm surface plasmons would increase the absorption of photons in the Si solar cell due to the need to conserve momentum.

## 6.0 Remarks, Broader Implications, Limitations and Future Work for this study

In this study, the charge transport kinetics of both holes and electrons are found from one solar cell device during normal solar cell operation. The carrier kinetics had to previously be found using transistors, hall effect measurements, or through current decay measurements based off of the solar cell geometry. Transistor and Hall effect measurement can acquire transport information about both holes and electrons however the conditions of the measurement do not match to the conditions of carrier transport in solar cells. Only one type of carrier can be determined in traditional current decay measurements based off the geometry of the device. Using a Dual illumination current decay measurement scheme, the kinetics of both holes and electrons during solar cell operation can be found. Using this technique, the hole and electron transport coefficients of P and N type PbS have been found. The kinetics of charge carriers with the addition of a P/N junction in PbS device was also studied. The result of this study found that in N type PbS films hole and electrons have similar transport properties where in P type PbS films electron transport is much slower than hole transport. With the addition of a P/N junction, hole and electron transport was significantly improved due to the addition of a drift region in the middle of the active layer of the device. The difference between hole and electron transport was minimized in high ratio of P to N type PbS films due to the drift region.

Broader implications: using the dual illumination scheme, other types of solar cell devices can be tested to determine their hole and electron kinetics. This would require a redesign of solar cell devices to utilize the dual illumination technique as two transparent electrodes are necessary for the measurement. Using this data, the geometry of solar cells can be designed to minimize

charge transport distances for the slower carrier. In the P type PbS case, the distances electrons must travel should be maximized so FTO illumination is optimal.

Limitations: quantitative numbers for PbS devices may only be pertinent to devices fabricated in this lab or using the same ligand exchange techniques. Quantum dot film fabrication is highly variable with many different contaminants, ligand exchange procedures, leading to different interparticle film spacing and donor densities may change if incomplete ligand exchange occurs.

Future work: Determine if other solar cell types can be analyzed in the same way such as perovskite, or other older technologies such as silicon or CdTe devices. For quantum dot devices, future work can be done to determine how different passivation techniques can change the electron and hole mobility in solar cell devices.

We have shown the addition of a Bragg mirror under a thin gold film will generate Tamm surface plasmons for photons at the Bragg wavelength. The Tamm surface plasmons increase the light absorption of PbS quantum dot solar cell devices that have fabricated in intimate contact with the plasmonic thin films. This in turn increased the quantum efficiency of the PbS solar cells and increases its extracted current. The Tamm surface plasmon effect can be widely tuned across the absorption spectra of the PbS active layer. We have found that by tuning the Bragg wavelength to match the area of lowest light absorbance of the PbS film, the most improvement in light absorption and device performance occurs. The plasmonic effect increases the local light absorbance of the film and can be found to improve the IPCE of solar cells with very thin active layer.

Broader impacts: Using Tamm surface plasmons in conjunction with solar cell devices can have a large impact on solar cell fabrication and use. Using Tamm surface plasmons to help absorb light in a semiconductor film can reduce the amount of material needed for solar cell fabrication and reduce recombination as the semiconductor film can be thinner and still absorb the majority of light. This can be applied to traditional solar cell devices such as Si, CdTe, or emerging photovoltaics like perovskite or organic solar cell devices.

Limitations: The Tamm surface plasmon does not improve the quantum efficiency of solar cell devices if the photon energy at which surface plasmon resonance occurs is lower than the bandgap of the solar cell active layer. This study does not determine if the increase of light absorption by Tamm surface plasmons can be applied to indirect bandgap materials that require a change in momentum and energy in electrons where direct bandgap materials only require a change in energy. The high processing temperatures of the Bragg mirror/ low temperature tolerance of the gold metal film may reduce the applicability of the thin film.

Future work: Tamm surface plasmons may be applied to non-quantum dot solar cells such as Si or CdTe. Changing the metal to other plasmonic compatible metals such as aluminum or silver may open up options for other applications. The work function of gold is not positioned for Olmec contacts will all semiconductors. A limitation of this design with using $TiO_2$ as a high refractive index layer. The refractive index of sputtered $TiO_2$ is heavily dependent on density and therefore deposition temperature. Using a high refractive index material that could be deposited at low temperatures will allow for the Tamm surface plasmon film to be deposited on solar cells rather than solar cells being deposited on the Tamm surface plasmon film.

## Bibliography


[1] A. Haines, R.S. Kovats, D. Campbell-Lendrum, C. Corvalan, Public Health, 120 (2006) 585-596.

[2] A. Miranda, in: D. Time (Ed.), 2018.

[3] I. Dincer, Energy Sources, 20 (1998) 427-453.

[4] I. Dincer, Renewable and Sustainable Energy Reviews, 4 (2000) 157-175.

[5] R.E.H. Sims, Solar Energy, 76 (2004) 9-17.

[6] BP, BP Statistical Review of World Energy 2016, (2015).

[7] P.K. Nayak, S. Mahesh, H.J. Snaith, D. Cahen, Nature Reviews Materials, 4 (2019) 269-285.

[8] K. Sopian, S.L. Cheow, S.H. Zaidi, AIP Conference Proceedings, 1877 (2017) 020004.

[9] Y. Masafumi, L. Kan-Hua, A. Kenji, K. Nobuaki, Journal of Physics D: Applied Physics, 51 (2018) 133002.

[10] E. H. Sargent, Advanced Materials, 17 (2005) 515-522.

[11] C.-H.M. Chuang, P.R. Brown, V. Bulović, M.G. Bawendi, Nature Materials, 13 (2014) 796.

[12] R.D. Schaller, V.I. Klimov, Physical Review Letters, 92 (2004) 186601.

[13] J.B. Sambur, T. Novet, B.A. Parkinson, Science, 330 (2010) 63.

[14] M. Liu, O. Voznyy, R. Sabatini, F.P. García de Arquer, R. Munir, Ahmed H. Balawi, X. Lan, F. Fan, G. Walters, Ahmad R. Kirmani, S. Hoogland, F. Laquai, A. Amassian, Edward H. Sargent, Nature Materials, 16 (2016) 258.

[15] L. Jingjing, Y. Yao, X. Shaoqing, G. Xiaofeng, Journal of Physics D: Applied Physics, 51 (2018) 123001.

[16] M.J. Madou, Fundamentals of microfabrication and nanotechnology. Solid-state physics, fluidics, and analytical techniques in micro- and nanotechnology, Third edition. Boca Raton, FL : CRC Press, [2012] ©2012, 2012.

[17] R.E. Hummel, Electronic Properties of Materials, 4 ed., Springer-Verlag New York, 2011.

[18] D.J. Wagner, Rensselaer Polytechnic Institute. , 2003.
[19] J. Kurpiers, D.M. Balazs, A. Paulke, S. Albrecht, I. Lange, L. Protesescu, M.V. Kovalenko, M.A. Loi, D. Neher, Applied Physics Letters, 108 (2016) 103102.

[20] A. Abete, G. Ferraro, Solar Cells, 28 (1990) 335-342.

[21] A. Ortiz-Conde, F. García-Sánchez, J. Muci, A. Sucre-González, Facta Universitatis, Series: Electronics and Energetics., 27 (2014) 57-102.

[22] T.J. McMahon, T.S. Basso, S.R. Rummel, Conference Record of the Twenty Fifth IEEE Photovoltaic Specialists Conference - 1996, 1996, pp. 1291-1294.

[23] E.L. Meyer, E.E.v. Dyk, Conference Record of the Thirty-first IEEE Photovoltaic Specialists Conference, 2005., 2005, pp. 1331-1334.

[24] T. Stubhan, T. Ameri, M. Salinas, J. Krantz, F. Machui, M. Halik, C.J. Brabec, Applied Physics Letters, 98 (2011) 253308.

[25] M.K. El-Adawi, I.A. Al-Nuaim, Vacuum, 64 (2001) 33-36.

[26] D. Pysch, A. Mette, S.W. Glunz, Solar Energy Materials and Solar Cells, 91 (2007) 1698-1706.

[27] K. Bouzidi, M. Chegaar, A. Bouhemadou, Solar Energy Materials and Solar Cells, 91 (2007) 1647-1651.

[28] H. Norde, Journal of Applied Physics, 50 (1979) 5052-5053.

[29] T. Trupke, E. Pink, R.A. Bardos, M.D. Abbott, Applied Physics Letters, 90 (2007) 093506.

[30] R.J. Handy, Solid-State Electronics, 10 (1967) 765-775.

[31] S.E. Shaheen, C.J. Brabec, N.S. Sariciftci, F. Padinger, T. Fromherz, J.C. Hummelen, Applied Physics Letters, 78 (2001) 841-843.

[32] C. Yasuo, I. Ashraful, W. Yuki, K. Ryoichi, K. Naoki, H. Liyuan, Japanese Journal of Applied Physics, 45 (2006) L638.

[33] J. Burschka, N. Pellet, S.-J. Moon, R. Humphry-Baker, P. Gao, M.K. Nazeeruddin, M. Grätzel, Nature, 499 (2013) 316.

[34] S.H. Park, A. Roy, S. Beaupré, S. Cho, N. Coates, J.S. Moon, D. Moses, M. Leclerc, K. Lee, A.J. Heeger, Nature Photonics, 3 (2009) 297.

[35] A.J. Nozik, Physica E: Low-dimensional Systems and Nanostructures, 14 (2002) 115-120.

[36] I. Mora-Sero, L. Bertoluzzi, V. Gonzalez-Pedro, S. Gimenez, F. Fabregat-Santiago, K.W. Kemp, E.H. Sargent, J. Bisquert, Nature Communications, 4 (2013) 2272.

[37] J.-Y. Kim, J. Yang, J.H. Yu, W. Baek, C.-H. Lee, H.J. Son, T. Hyeon, M.J. Ko, ACS Nano, 9 (2015) 11286-11295.

[38] M.L. Böhm, T.C. Jellicoe, M. Tabachnyk, N.J.L.K. Davis, F. Wisnivesky-Rocca-Rivarola, C. Ducati, B. Ehrler, A.A. Bakulin, N.C. Greenham, Nano Letters, 15 (2015) 7987-7993.

[39] H.J. Yun, T. Paik, M.E. Edley, J.B. Baxter, C.B. Murray, ACS Applied Materials & Interfaces, 6 (2014) 3721-3728.

[40] L. Hu, S. Huang, R. Patterson, J.E. Halpert, Journal of Materials Chemistry C, 7 (2019) 4497-4502.

[41] K.S. Jeong, J. Tang, H. Liu, J. Kim, A.W. Schaefer, K. Kemp, L. Levina, X. Wang, S. Hoogland, R. Debnath, L. Brzozowski, E.H. Sargent, J.B. Asbury, ACS Nano, 6 (2012) 89-99.

[42] K.A. Sablon, A. Sergeev, N. Vagidov, J.W. Little, V. Mitin, Solar Energy Materials and Solar Cells, 117 (2013) 638-644.

[43] S. Nakade, T. Kanzaki, Y. Wada, S. Yanagida, Langmuir, 21 (2005) 10803-10807.

[44] V. Ranjan, C.S. Solanki, R.K. Lal, 2008 2nd National Workshop on Advanced Optoelectronic Materials and Devices, 2008, pp. 299-306.

[45] A. Zaban, M. Greenshtein, J. Bisquert, ChemPhysChem, 4 (2003) 859-864.

[46] D.W. de Quilettes, S.M. Vorpahl, S.D. Stranks, H. Nagaoka, G.E. Eperon, M.E. Ziffer, H.J. Snaith, D.S. Ginger, Science, 348 (2015) 683.

[47] J.E. Mahan, T.W. Ekstedt, R.I. Frank, R. Kaplow, IEEE Transactions on Electron Devices, 26 (1979) 733-739.

[48] J. Tae-Won, F.A. Lindholm, A. Neugroschel, IEEE Transactions on Electron Devices, 31 (1984) 588-595.

[49] A.P. Alivisatos, Science, 271 (1996) 933.

[50] D. Bera, L. Qian, T.-K. Tseng, P.H. Holloway, Materials, 3 (2010).

[51] O.E. Semonin, J.M. Luther, M.C. Beard, Materials Today, 15 (2012) 508-515.

[52] W.R. Algar, A.J. Tavares, U.J. Krull, Analytica Chimica Acta, 673 (2010) 1-25.

[53] G.H. Carey, A.L. Abdelhady, Z. Ning, S.M. Thon, O.M. Bakr, E.H. Sargent, Chemical Reviews, 115 (2015) 12732-12763.

[54] J. Sun, W. Yu, A. Usman, T.T. Isimjan, S. Dgobbo, E. Alarousu, K. Takanabe, O.F. Mohammed, The Journal of Physical Chemistry Letters, 5 (2014) 659-665.

[55] Y. Yang, W. Rodríguez-Córdoba, T. Lian, Nano Letters, 12 (2012) 4235-4241.

[56] O.E. Semonin, J.M. Luther, S. Choi, H.-Y. Chen, J. Gao, A.J. Nozik, M.C. Beard, Science, 334 (2011) 1530-1533.

[57] A.G. Midgett, J.M. Luther, J.T. Stewart, D.K. Smith, L.A. Padilha, V.I. Klimov, A.J. Nozik, M.C. Beard, Nano Letters, 13 (2013) 3078-3085.

[58] W. Yoon, J.E. Boercker, M.P. Lumb, D. Placencia, E.E. Foos, J.G. Tischler, Scientific Reports, 3 (2013) 2225.

[59] H. Wang, T. Kubo, J. Nakazaki, T. Kinoshita, H. Segawa, The Journal of Physical Chemistry Letters, 4 (2013) 2455-2460.

[60] Z. Zhang, C. Shi, J. Chen, G. Xiao, L. Li, Applied Surface Science, 410 (2017) 8-13.

[61] A.G. Shulga, L. Piveteau, S.Z. Bisri, M.V. Kovalenko, M.A. Loi, Advanced Electronic Materials, 2 (2016) 1500467.

[62] G.H. Carey, L. Levina, R. Comin, O. Voznyy, E.H. Sargent, Advanced Materials, 27 (2015) 3325-3330.

[63] I.J. Kramer, G. Moreno-Bautista, J.C. Minor, D. Kopilovic, E.H. Sargent, Applied Physics Letters, 105 (2014) 163902.

[64] P. Guyot-Sionnest, The Journal of Physical Chemistry Letters, 3 (2012) 1169-1175.

[65] H. Wang, Y. Wang, B. He, W. Li, M. Sulaman, J. Xu, S. Yang, Y. Tang, B. Zou, ACS Applied Materials & Interfaces, 8 (2016) 18526-18533.

[66] Y. Cho, B. Hou, J. Lim, S. Lee, S. Pak, J. Hong, P. Giraud, A.R. Jang, Y.-W. Lee, J. Lee, J.E. Jang, H.J. Snaith, S.M. Morris, J.I. Sohn, S. Cha, J.M. Kim, ACS Energy Letters, 3 (2018) 1036-1043.

[67] R.S. Allgaier, W.W. Scanlon, Physical Review, 111 (1958) 1029-1037.

[68] G.H. Carey, A.L. Abdelhady, Z. Ning, S.M. Thon, O.M. Bakr, E.H. Sargent, Chem Rev, 115 (2015) 12732-12763.

[69] M.A. Hines, G.D. Scholes, Advanced Materials, 15 (2003) 1844-1849.

[70] P.R. Brown, D. Kim, R.R. Lunt, N. Zhao, M.G. Bawendi, J.C. Grossman, V. Bulović, ACS Nano, 8 (2014) 5863-5872.

[71] B. Kundu, A.J. Pal, The Journal of Physical Chemistry C, 122 (2018) 11570-11576.

[72] S.Z. Bisri, C. Piliego, M. Yarema, W. Heiss, M.A. Loi, Advanced Materials, 25 (2013) 4309-4314.

[73] N. Ray, N.E. Staley, D.D.W. Grinolds, M.G. Bawendi, M.A. Kastner, Nano Letters, 15 (2015) 4401-4405.

[74] D.M. Balazs, D.N. Dirin, H.-H. Fang, L. Protesescu, G.H. ten Brink, B.J. Kooi, M.V. Kovalenko, M.A. Loi, ACS Nano, 9 (2015) 11951-11959.

[75] C.R. Kagan, E. Lifshitz, E.H. Sargent, D.V. Talapin, Science, 353 (2016).

[76] S. Pradhan, A. Stavrinadis, S. Gupta, Y. Bi, F. Di Stasio, G. Konstantatos, Small, 13 (2017).

[77] D.M. Balazs, K.I. Bijlsma, H.-H. Fang, D.N. Dirin, M. Döbeli, M.V. Kovalenko, M.A. Loi, Science Advances, 3 (2017) eaao1558.

[78] Y. Kim, H. Ko, B. Park, Journal of Physics D: Applied Physics, 51 (2018) 145306.

[79] Z. Ning, O. Voznyy, J. Pan, S. Hoogland, V. Adinolfi, J. Xu, M. Li, A.R. Kirmani, J.-P. Sun, J. Minor, K.W. Kemp, H. Dong, L. Rollny, A. Labelle, G. Carey, B. Sutherland, I. Hill, A. Amassian, H. Liu, J. Tang, O.M. Bakr, E.H. Sargent, Nature Materials, 13 (2014) 822.

[80] W.-k. Koh, A.Y. Koposov, J.T. Stewart, B.N. Pal, I. Robel, J.M. Pietryga, V.I. Klimov, Scientific Reports, 3 (2013) 2004.

[81] D. Mocatta, G. Cohen, J. Schattner, O. Millo, E. Rabani, U. Banin, Science, 332 (2011) 77.

[82] M. Shim, P. Guyot-Sionnest, Nature, 407 (2000) 981.

[83] H.-J. Lin, S. Vedraine, J. Le-Rouzo, S.-H. Chen, F. Flory, C.-C. Lee, Solar Energy Materials and Solar Cells, 117 (2013) 652-656.

[84] S. Chen, Y.j. Wang, Q. Liu, G. Shi, Z. Liu, K. Lu, L. Han, X. Ling, H. Zhang, S. Cheng, W. Ma, Advanced Energy Materials, 8 (2018) 1701194.

[85] Y.A. Akimov, W.S. Koh, Plasmonics, 6 (2011) 155-161.

[86] P. Jain, A. Palakkandy, Improved Efficiency of Plasmonic Tin Sulfide Solar Cells, 2015.

[87] S. Link, M.A. El-Sayed, The Journal of Physical Chemistry B, 103 (1999) 4212-4217.

[88] B. Ding, B.J. Lee, M. Yang, H.S. Jung, J.-K. Lee, Advanced Energy Materials, 1 (2011) 415-421.

[89] J.W.L. Eccles, U. Bangert, M. Bromfield, P. Christian, A.J. Harvey, P. Thomas, Journal of Physics: Conference Series, 241 (2010) 012090.

[90] B. Ding, T. Gao, Y. Wang, D.H. Waldeck, P.W. Leu, J.-K. Lee, Solar Energy Materials and Solar Cells, 128 (2014) 386-393.

[91] T. Kawawaki, H. Wang, T. Kubo, K. Saito, J. Nakazaki, H. Segawa, T. Tatsuma, ACS Nano, 9 (2015) 4165-4172.

[92] P. Mandal, S. Sharma, Renewable and Sustainable Energy Reviews, 65 (2016) 537-552.

[93] S. Exarhos, A. Alvarez-Barragan, E. Aytan, A.A. Balandin, L. Mangolini, ACS Energy Letters, 3 (2018) 2349-2356.

[94] A. Juneau-Fecteau, L.G. Fréchette, Optical Materials Express, 8 (2018) 2774.

[95] M. Parente, S. Sheikholeslami, G.V. Naik, J.A. Dionne, A. Baldi, The Journal of Physical Chemistry C, 122 (2018) 23631-23638.

[96] M.K. Shukla, R. Das, Opt Lett, 43 (2018) 362-365.

[97] H.A. Atwater, A. Polman, Plasmonics for improved photovoltaic devices, Materials for Sustainable Energy, pp. 1-11.

[98] M.L. Brongersma, V.M. Shalaev, Science, 328 (2010) 440-441.

[99] M.S. Tame, K.R. McEnery, Ş.K. Özdemir, J. Lee, S.A. Maier, M.S. Kim, Nature Physics, 9 (2013) 329.

[100] D.K. Gramotnev, S.I. Bozhevolnyi, Nature Photonics, 4 (2010) 83-91.

[101] M. Kaliteevski, I. Iorsh, S. Brand, R.A. Abram, J.M. Chamberlain, A.V. Kavokin, I.A. Shelykh, Physical Review B, 76 (2007).

[102] M.E. Sasin, R.P. Seisyan, M.A. Kalitteevski, S. Brand, R.A. Abram, J.M. Chamberlain, A.Y. Egorov, A.P. Vasil'ev, V.S. Mikhrin, A.V. Kavokin, Applied Physics Letters, 92 (2008) 251112.

[103] M.E. Sasin, R.P. Seisyan, M.A. Kaliteevski, S. Brand, R.A. Abram, J.M. Chamberlain, I.V. Iorsh, I.A. Shelykh, A.Y. Egorov, A.P. Vasil'ev, V.S. Mikhrin, A.V. Kavokin, Superlattices and Microstructures, 47 (2010) 44-49.

[104] X.-L. Zhang, J.-F. Song, X.-B. Li, J. Feng, H.-B. Sun, Applied Physics Letters, 101 (2012) 243901.

[105] I.Y. Chestnov, E.S. Sedov, S.V. Kutrovskaya, A.O. Kucherik, S.M. Arakelian, A.V. Kavokin, Physical Review B, 96 (2017) 245309.

[106] T.-y. Chung, A. Rapaport, V. Smirnov, L.B. Glebov, M.C. Richardson, M. Bass, Opt. Lett., 31 (2006) 229-231.

[107] C.J.R. Sheppard, Pure and Applied Optics: Journal of the European Optical Society Part A, 4 (1995) 665.

[108] J. Matsuoka, N. Kitamura, S. Fujinaga, T. Kitaoka, H. Yamashita, Journal of Non-Crystalline Solids, 135 (1991) 86-89.

[109] D. Mergel, D. Buschendorf, S. Eggert, R. Grammes, B. Samset, Thin Solid Films, 371 (2000) 218-224.

[110] D.E. Bornside, C.W. Macosko, L.E. Scriven, Journal of imaging technology, 13 (1987) 122-130.

[111] L.E. Scriven, MRS Proceedings, 121 (2011) 717.

[112] P. Sigmund, Physical Review, 184 (1969) 383-416.

[113] H.R. Koenig, L.I. Maissel, IBM Journal of Research and Development, 14 (1970) 168-171.

[114] R.K. Waits, Journal of Vacuum Science and Technology, 15 (1978) 179-187.

[115] S. Berg, H.O. Blom, T. Larsson, C. Nender, Journal of Vacuum Science & Technology A, 5 (1987) 202-207.

[116] P.F. Carcia, R.S. McLean, M.H. Reilly, G. Nunes, Applied Physics Letters, 82 (2003) 1117-1119.

[117] S. Berg, T. Nyberg, Thin Solid Films, 476 (2005) 215-230.

[118] W.D. Sproul, D.J. Christie, D.C. Carter, Thin Solid Films, 491 (2005) 1-17.

[119] C.V. Ramana, O.M. Hussain, B.S. Naidu, P.J. Reddy, Thin Solid Films, 305 (1997) 219-226.

[120] J. George, C.S. Menon, Surface and Coatings Technology, 132 (2000) 45-48.

[121] A. Tanuševski, D. Poelman, Solar Energy Materials and Solar Cells, 80 (2003) 297-303.

[122] M. Leskelä, M. Ritala, Thin Solid Films, 409 (2002) 138-146.

[123] B.S. Lim, A. Rahtu, R.G. Gordon, Nature Materials, 2 (2003) 749-754.

[124] S.M. George, Chemical Reviews, 110 (2010) 111-131.

[125] J.B. Kim, D.R. Kwon, K. Chakrabarti, C. Lee, K.Y. Oh, J.H. Lee, Journal of Applied Physics, 92 (2002) 6739-6742.

[126] S.D. Elliott, G. Scarel, C. Wiemer, M. Fanciulli, G. Pavia, Chemistry of Materials, 18 (2006) 3764-3773.

[127] D.N. Goldstein, J.A. McCormick, S.M. George, The Journal of Physical Chemistry C, 112 (2008) 19530-19539.

[128] S.M. Rossnagel, A. Sherman, F. Turner, Journal of Vacuum Science & Technology B: Microelectronics and Nanometer Structures Processing, Measurement, and Phenomena, 18 (2000) 2016-2020.

[129] J.-S. Park, M.-J. Lee, C.-S. Lee, S.-W. Kang, Electrochemical and Solid-State Letters, 4 (2001) C17-C19.

[130] B. Hoex, S.B.S. Heil, E. Langereis, M.C.M. van de Sanden, W.M.M. Kessels, Applied Physics Letters, 89 (2006) 042112.

[131] H.B. Profijt, S.E. Potts, M.C.M. van de Sanden, W.M.M. Kessels, Journal of Vacuum Science & Technology A, 29 (2011) 050801.

[132] C. Rost, S. Karg, W. Riess, M.A. Loi, M. Murgia, M. Muccini, Applied Physics Letters, 85 (2004) 1613-1615.

[133] A.J. Shields, M.P. O'Sullivan, I. Farrer, D.A. Ritchie, R.A. Hogg, M.L. Leadbeater, C.E. Norman, M. Pepper, Applied Physics Letters, 76 (2000) 3673-3675.

[134] D.V. Talapin, C.B. Murray, Science, 310 (2005) 86.

[135] T.P. Osedach, N. Zhao, T.L. Andrew, P.R. Brown, D.D. Wanger, D.B. Strasfeld, L.-Y. Chang, M.G. Bawendi, V. Bulović, ACS Nano, 6 (2012) 3121-3127.

[136] F. Hetsch, N. Zhao, S.V. Kershaw, A.L. Rogach, Materials Today, 16 (2013) 312-325.

[137] Y. Liu, J. Tolentino, M. Gibbs, R. Ihly, C.L. Perkins, Y. Liu, N. Crawford, J.C. Hemminger, M. Law, Nano Letters, 13 (2013) 1578-1587.

[138] M.I. Nugraha, R. Häusermann, S.Z. Bisri, H. Matsui, M. Sytnyk, W. Heiss, J. Takeya, M.A. Loi, Advanced Materials, 27 (2015) 2107-2112.

[139] A.G. Shulga, S. Kahmann, D.N. Dirin, A. Graf, J. Zaumseil, M.V. Kovalenko, M.A. Loi, ACS nano, 12 (2018) 12805-12813.

[140] S.M. Jung, H.L. Kang, J.K. Won, J. Kim, C. Hwang, K. Ahn, I. Chung, B.-K. Ju, M.-G. Kim, S.K. Park, ACS Applied Materials & Interfaces, 10 (2018) 3739-3749.

[141] S. Kahmann, A. Shulga, M.A. Loi, Advanced Functional Materials, 0 (2019) 1904174.

[142] A. Einstein, Annalen der Physik, 322 (1905) 549-560.

[143] X.-L. Zhang, J.-F. Song, X.-B. Li, J. Feng, H.-B. Sun, Organic Electronics, 14 (2013) 1577-1585.